A PLATFORM FOR PROACTIVE, RISK-BASED SLOPE ASSET MANAGEMENT, PHASE II

FINAL PROJECT REPORT

by

Keith Cunningham, PI - University of Alaska Fairbanks
Michael Olsen, Co PI – Oregon State University Joseph Wartman, Co-PI – University of Washington
Lisa Dunham – University of Washington

Sponsorship
(Alaska University Transportation Center, Alaska Department of Transportation)

for

Pacific Northwest Transportation Consortium (PacTrans)
USDOT University Transportation Center for Federal Region 10
University of Washington
More Hall 112, Box 352700
Seattle, WA 98195-2700

In cooperation with US Department of Transportation-Research and Innovative Technology Administration (RITA)

Disclaimer

The contents of this report reflect the views of the authors, who are responsible for the facts and the accuracy of the information presented herein. This document is disseminated under the sponsorship of the U.S. Department of Transportation's University Transportation Centers Program, in the interest of information exchange. The Pacific Northwest Transportation Consortium, the U.S. Government and matching sponsor assume no liability for the contents or use thereof.

Technical Report Documentation Page

1. Report No.	2. Government Accession No.	3. Recipient's Catalog No.
2013-M-UAF-0042		

4. Title and Subtitle	5. Report Date
A Platform for Proactive Risk-Based Slope Asset Management – Phase II Final Project Report	8/31/2015
	6. Performing Organization Code

7. Author(s)	8. Performing Organization Report No.
Keith W. Cunningham – University of Alaska Michael Olsen – Oregon State University Joseph Wartman – University of Washington Lisa Dunham – University of Washington	

9. Performing Organization Name and Address	10. Work Unit No. (TRAIS)
PacTrans Pacific Northwest Transportation Consortium University Transportation Center for Region 10 University of Washington More Hall 112 Seattle, WA 98195-2700	11. Contract or Grant No. DTRT12-UTC10

12. Sponsoring Organization Name and Address	13. Type of Report and Period Covered
United States of America Department of Transportation Research and Innovative Technology Administration	Research 11/01/2013-8/31/2015
	14. Sponsoring Agency Code

15. Supplementary Notes

Report uploaded at www.pacTrans.org

16. Abstract

The lidar visualization technique developed by this project enables highway managers to understand changes in slope characteristics along highways. This change detection and analysis can be the basis of informed decisions for slope inspection and remediation. Mitigating unstable slopes and their associated hazards reduce threats to safety and regional commerce while better allocating resources.

17. Key Words: Research management (Cw), Planning (Ep), Innovation (Ey), Maintenance practices (Fmb), Mathematical analysis (Uh), Geometry (Up), Statistical analysis (Us), Risk (Hk), Risk assessment (Hka), Alaska, Asset management, GIS, Slope stability, Laser scanning, Lidar, Mobile Mapping, Risk-based, Rockfall energy index, Evaluate, Highway	18. Distribution Statement No restrictions.

19. Security Classification (of this report)	20. Security Classification (of this page)	21. No. of Pages 73	22. Price
Unclassified.	Unclassified.		NA

Form DOT F 1700.7 (8-72) **Reproduction of completed page authorized**

METRIC (SI*) CONVERSION FACTORS

APPROXIMATE CONVERSIONS TO SI UNITS

Symbol	When You Know	Multiply By	To Find	Symbol
		LENGTH		
in	inches	25.4		mm
ft	feet	0.3048		m
yd	yards	0.914		m
mi	Miles (statute)	1.61		km
		AREA		
in^2	square inches	645.2	millimeters squared	cm^2
ft^2	square feet	0.0929	meters squared	m^2
yd^2	square yards	0.836	meters squared	m^2
mi^2	square miles	2.59	kilometers squared	km^2
ac	acres	0.4046	hectares	ha
		MASS (weight)		
oz	Ounces (avdp)	28.35	grams	g
lb	Pounds (avdp)	0.454	kilograms	kg
T	Short tons (2000 lb)	0.907	megagrams	mg
		VOLUME		
fl oz	fluid ounces (US)	29.57	milliliters	mL
gal	Gallons (liq)	3.785	liters	liters
ft^3	cubic feet	0.0283	meters cubed	m^3
yd^3	cubic yards	0.765	meters cubed	m^3
		TEMPERATURE (exact)		
ºF	Fahrenheit temperature	5/9 (ºF-32)	Celsius temperature	ºC
		ILLUMINATION		
fc	Foot-candles	10.76	lux	lx
fl	foot-lamberts	3.426	candela/m^2	cd/cm^2
		FORCE and PRESSURE or STRESS		
lbf	pound-force	4.45	newtons	N
psi	pound-force per square inch	6.89	kilopascals	kPa

Note: Volumes greater than 1000 L shall be shown in m^3

These factors conform to the requirement of FHWA Order 5190.1A *SI is the symbol for the International System of Measurements

APPROXIMATE CONVERSIONS FROM SI UNITS

Symbol	When You Know	Multiply By	To Find	Symbol
		LENGTH		
mm	millimeters	0.039	inches	in
m	meters	3.28	feet	ft
m	meters	1.09	yards	yd
km	kilometers	0.621	Miles (statute)	mi
		AREA		
mm^2	millimeters squared	0.0016	square inches	in^2
m^2	meters squared	10.764	square feet	ft^2
km^2	kilometers squared	0.39	square miles	mi^2
ha	hectares (10,000 m^2)	2.471	acres	ac
		MASS (weight)		
g	grams	0.0353	Ounces (avdp)	oz
kg	kilograms	2.205	Pounds (avdp)	lb
mg	megagrams (1000 kg)	1.103	short tons	T
		VOLUME		
mL	milliliters	0.034	fluid ounces (US)	fl oz
liters	liters	0.264	Gallons (liq)	gal
m^3	meters cubed	35.315	cubic feet	ft^3
m^3	meters cubed	1.308	cubic yards	yd^3
		TEMPERATURE (exact)		
ºC	Celsius temperature	9/5 ºC+32	Fahrenheit temperature	ºF
		ILLUMINATION		
lx	lux	0.0929	foot-candles	fc
cd/cm^2	candela/m^2	0.2919	foot-lamberts	fl
		FORCE and PRESSURE or STRESS		
N	newtons	0.225	pound-force	lbf
kPa	kilopascals	0.145	pound-force per square inch	psi

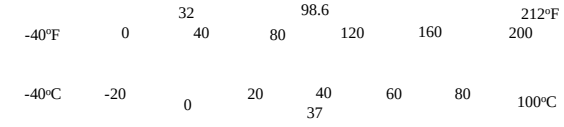

Table of Contents

List of Figures

List of Tables

List of Abbreviations

AK DOT&PF: Alaska Department of Transportation & Public Facilities

ASCII: American Standard Code for Information Interchange

DEM: Digital Elevation Model

DMI: Distance Measurement Indicator

DSM: Digital Surface Model

DTM: Digital Terrain Model

FHWA: Federal Highway Administration

GAM: Geotechnical Asset Management

GIS: Geographic Information System

GNSS: Global Navigation Satellite System

GPS: Global Positioning System

Hz: Hertz

IMU: Inertial Measurement Unit

INS: Inertial Navigation System

KE: Kinetic Energy

KMZ: Zipped KML (Keyhole Markup Language)

Lidar: Light Detection and Ranging

MAP 21: Moving Ahead for Progress in the 21st Century Act

MSE: Mechanically Stabilized Earth

MLS: Mobile Laser Scan or Mobile LiDAR System

MP: Mile Post

NCHRP: National Cooperative Highway Research Program

OLS: Ordinary Least Squares

ODR: Orthogonal Distance Regression

PacTrans: Pacific Northwest Transportation Consortium

PBV: Point Bounding-Box Vertex

RAI: Rockslope Activity Index

RDA: Rockslope Deterioration Assessment

RGB: Red Green Blue

RHRS: Rockfall Hazard Rating System

RINEX: Receiver Independent Exchange

RMS: Root Mean Square

RTK: Real Time Kinematic

TAM: Transportation Asset Management

TIN: Triangulated Irregular Network

TLS: Terrestrial Laser Scan

TRB: Transportation Research Board

WSDOT: Washington State Department of Transportation

XYZ: Cartesian coordinates with three dimensional, orthogonal axes

XYZRGBI: XYZ coordinates with RGB color values and Intensity value

Abstract

The lidar visualization technique this project has developed enables highway managers to understand changes in slope characteristics along highways. This change detection and analysis can inform decisions for slope inspection and remediation. Mitigating unstable slopes and their associated hazards reduce threats to safety and regional commerce, and enables resources to be better allocated.

Executive Summary

Unstable slopes along transportation corridors are a long-term concern of highway managers. Although events such as rock falls and landslides may occur infrequently, they present significant safety risks and can negatively impact regional commerce. This same infrequency often results in complacent slope management, especially with respect to budgeting for preventative solutions. And because most slopes are laborious and costly to monitor over time, many of the Decision Support Systems that drive proactive Transportation Asset Management initiatives have not been implemented.

Lidar (light detection and ranging) laser scanning permits the rapid assessment of slopes. Time-series lidar datasets enables more confident slope asset management than the probabilistic studies based on landslide inventories that are currently used. Time-series lidar slope analysis enables a proactive approach to visualize slope instability.

Major findings for this research include the following:

1. Static terrestrial lidar scanning requires the operator to consider optimal locations for scanning.
2. Multiple lidar scans can be fused together to completely describe the slope of larger areas.
3. Multiple lidar scans from different times can be compared and analyzed for change. Visualizing slope change can help to identify and quantify areas of erosion and accretion.
4. Fusing imagery with the lidar scans supports the identification of geologic features that cannot be identified solely using lidar point cloud morphology.
5. Data filtering the lidar data is necessary to remove vegetation that obscures slope characteristics.

6. Change detection techniques, subtracting an earlier lidar surface from the current lidar surface can compute areas of change in the rock slope, as well as the volumetric change through time.
7. Volumetric change coupled with the change location (height on the slope) can be used to calculate the energy released by the slope through time.
8. The energy released at specific slope locations can be used to determine the risk associated with released rock on the slope and help plan mitigation strategies. This is the basis of the Rockfall Energy Index presented in Chapter Four.

Visualizing slope change results in a simple, yet powerful tool for analyzing slope risk and mitigation planning.

Chapter 1 Background and Study Site

This Phase II research project evaluated the tools and visualization methods used to quantify slope stability along highway corridors. The Phase I research examined traditional methods of characterizing unstable slopes, and then considered how those approaches could be further developed by utilizing the surface models generated with lidar laser scanning. For a detailed review of relevant literature, please see the Phase I report.

Lidar data in Phase I was collected first from a mobile platform, a moving truck, which enabled efficient data collection along the highways corridors in question. Unfortunately, the surface models obtained from quick mobile scanning were not sufficiently detailed for this study's goal of developing classification algorithms for identifying unstable slope sections, and evaluating slope change. However, the mobile platform will be more efficient for longer term studies, and will provide sufficient slope characterization information.

A second set of laser scans from static locations resulted in higher quality lidar data, but the differences in lidar sample density and resolution between the respective mobile and static data sets presented challenges in evaluating slope change. A second collection of static lidar scans was made in the second year of the Phase I project in order to make direct comparisons of the static laser scans at a higher resolution.

The Phase II project resulted in a third collection of static laser scans, and comparing three-year data sets enabled slope change to be determined. This helped the researchers understand not only the costs associated with the lidar data collection, but also the data processing and filtering required. The techniques developed are applicable to visualizing slope change, including erosion and accretion of sediment, talus, and other debris.

The aim of this project aligns with the strategic goals of **Safety, Cost Effectiveness,** and **Good Repair**. Slope failures (e.g., landslides) pose a hazard to public safety, particularly when they occur near public infrastructure. The debris from failed slopes can not only create impact hazards, but can also close down sections of highway for extended periods of time. This is particularly problematic when these incidents occur along critical transportation bottlenecks. Several highway corridors cross unstable terrain in the Coast Range of the Pacific Northwest and in many parts of Alaska, providing minimal alternatives for people to re-route in the event of a road closure. A proactive, performance-based approach to monitor slopes prior to catastrophic failure will enable improved decisions regarding appropriate maintenance repair and mitigation and will ensure improved allocation of the limited DOT resources.

This project also ties significantly into the MAP21 national performance goals: Safety, Infrastructure Condition, Congestion Reduction, System Reliability, Freight Movement and Economic Vitality, Environmental Sustainability, Reduced Project Delivery Delays. A key focus of the MAP21 legislation calls for use of advanced geospatial technologies to aid in asset management by transportation agencies.

Study Site

Researchers at the Pacific Northwest Transportation Consortium (PacTrans) selected two study areas with the assistance of geotechnical engineers at the Alaska Department of Transportation and Public Facilities (AKDOT&PF). The study sites are locations along highway corridors with unstable slopes.

The Glitter Gulch site is near the entrance of the Denali National Park, located between mileposts 239 and 247 on the Parks Highway. The second site, Long Lake, is situated between mileposts 78 to 89 on the Glenn Highway.

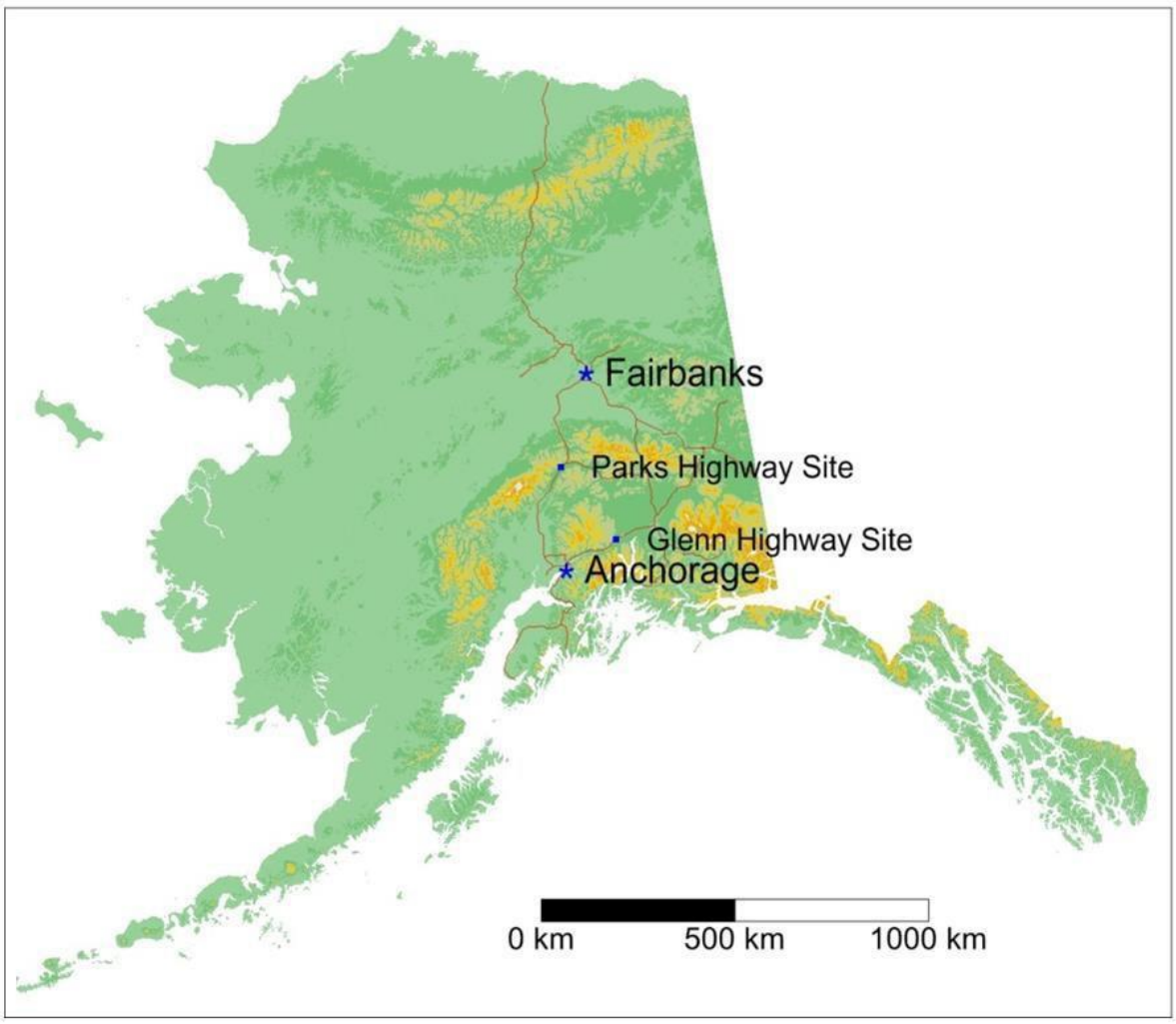

Figure 1 Map of Study Sites

Geologic Setting

Alaska largely consists of a number of accreted terranes, as shown in Figure 2. These terranes are the product of subduction, whereby the Pacific plate has acted as a conveyer belt for geologic material, bringing in portions of distinctly different rock that has become bound together by faults (Thornberry-Ehrlich 2010). The collision of these terranes with the existing

land mass has caused the uplift of mountains, volcanic activity, and seismicity that are associated with Alaska today.

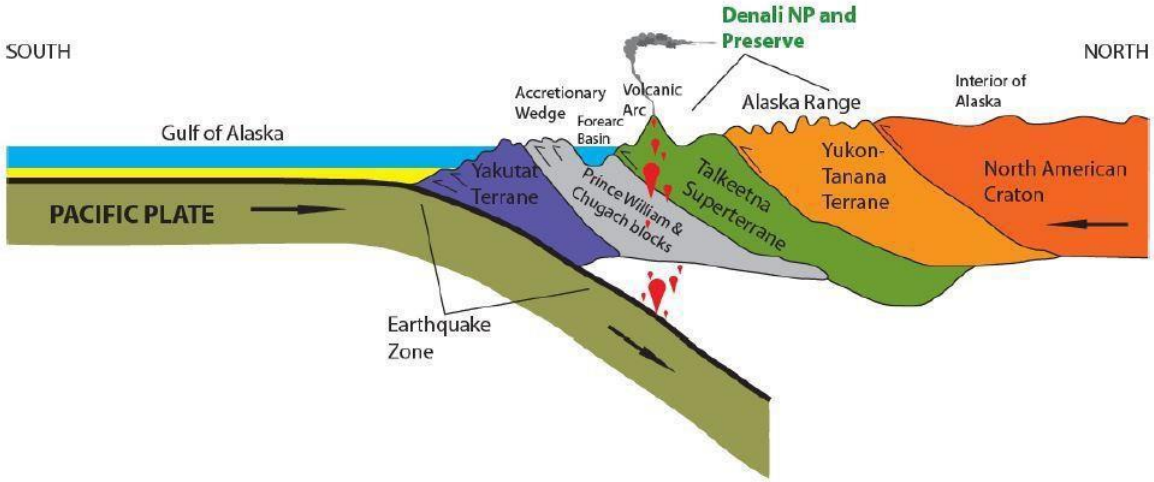

Figure 2 Alaska Terranes (Thornberry-Ehrlich 2010)

Glitter Gulch is located within the Yukon-Tanana Terrane, which is the oldest of the terranes comprising Alaska. This terrane is part of what is now known as the Alaska Range, a chain of mountains that extends east to west across southern Alaska, creating a drainage divide between the Cook Inlet and the Yukon lowlands (Thornberry-Ehrlich 2010). The Denali fault divides the Alaska Range, running approximately 20 miles (30 km) to the south of the study area, though the fault's seismic activity does not directly affect Glitter Gulch.

The main type of rock found within the Glitter Gulch study area is a rock is known as Birch Creek Schist, or Healy Schist, that Connor (1988) describes as "[a] metamorphic [rock], muscovite-quartz schist, micaceous quartz and lesser amounts of graphitic schist." Wahrhaftig (1958) notes that Birch Creek schist is inherently weak because of its "ease of separation along planes of foliation, produced by tiny, oriented mica flakes." This rock also includes cross-joints, which run near the vertical plane and may locally abut basalt dikes. Figure 3 is a geologic map of

the area that shows volcanic dikes (Tvim, Tvif) within the Healy schist (PzpCp). The volcanic rock can be clearly seen as the darker rock in Figure 4, with a lighter Healy schist layer below.

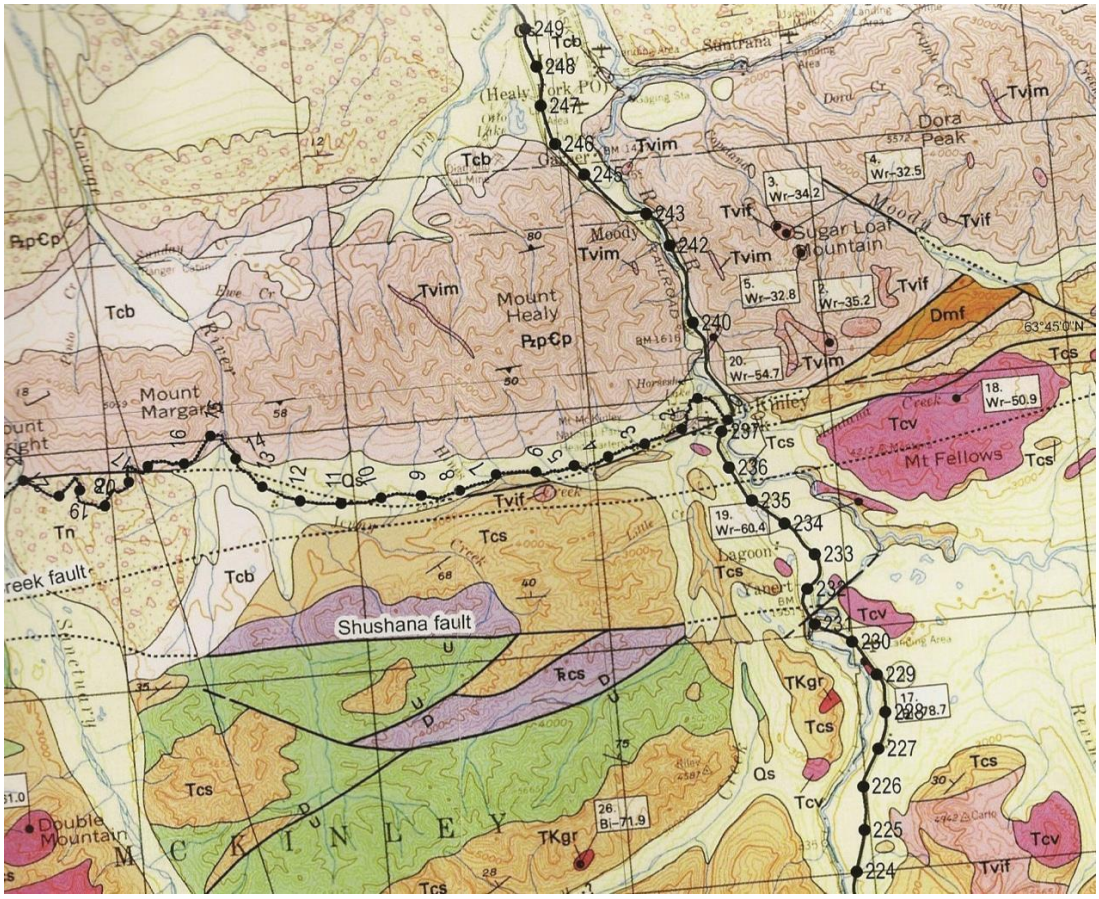

Figure 3 Geologic map of the Glitter Gulch area.

Figure 4 Glitter Gulch rock slope with darker basalt and lighter schist

The Long Lake site, which also lies within a region of accreted terrane, primarily consists of sedimentary rocks of the Matanuska and Chickaloon Formations. The Matanuska Formation is a marine sedimentary deposit formed during the orogenic rise of the Talkeetna Mountains. The Chickaloon Formation was deposited as propagating alluvial fans on top of the Matanuska Formation that formed as the Talkeetna Mountains were uplifted and sequentially eroded. (Belowich 2006) The Castle Mountain Fault runs parallel about 3 miles (5 km) north of the Long Lake; there is no evidence that it is active, nor that it affects the study area. The highway follows the glacial cut into the Chickaloon Formation; however, no other glacial evidence may be found in the area. (Trop 2006)

The Matanuska Formation is exposed in road cuts and rock outcrops around milepost 85, and largely consists of dark mudstones. The Chickaloon Formation is mainly carbonaceous siltstone, coal and sandstone and extends across the Long Lake site (Trop 2006). Mafic sill intrusions are located throughout the Matanuska and Chickaloon Formations. The general

geology of the Long Lake region is shown on Figure 5, with the dotted line indicating the location of the Glenn Highway.

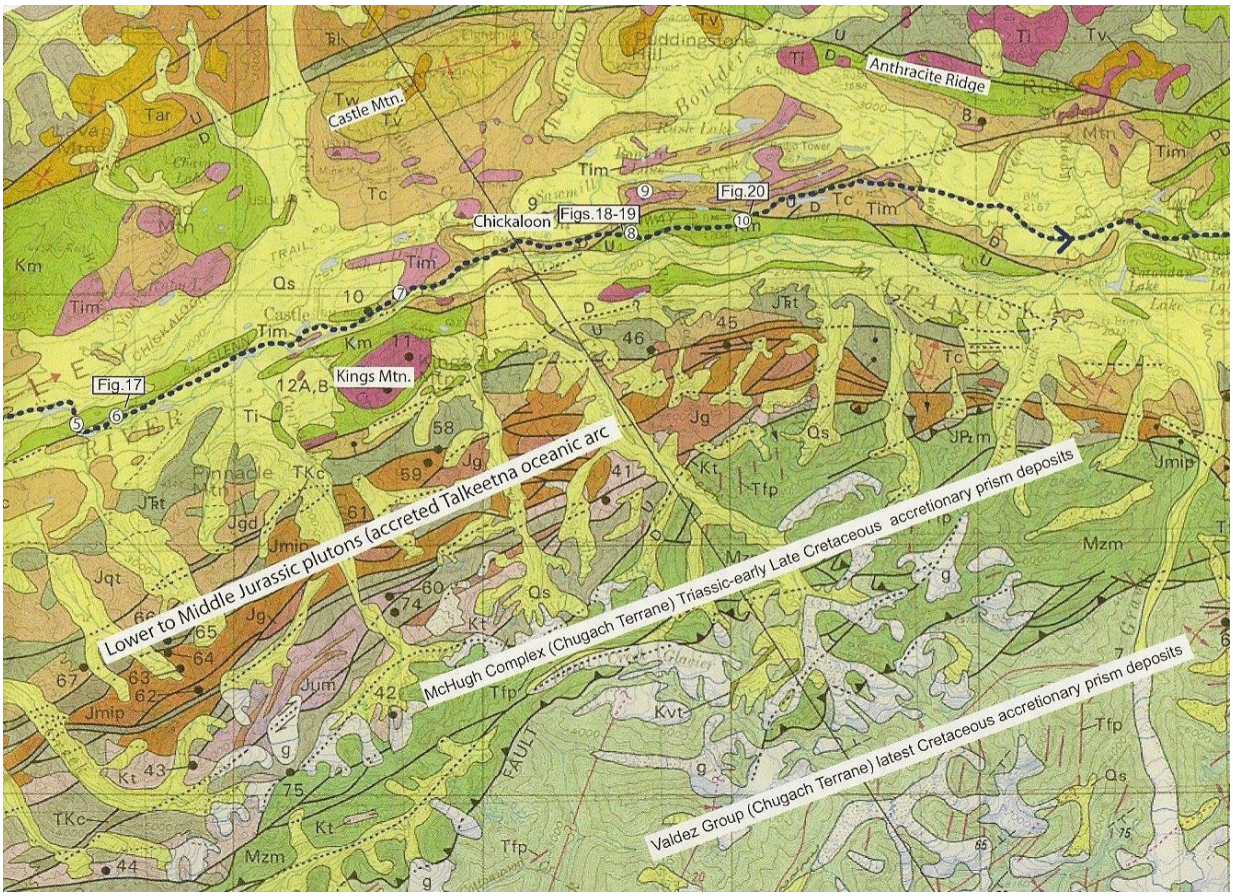

Figure 5 Geologic Map of the Long Lake site

Table 1 summarizes the climate of the Glitter Gulch and Long Lake regions. Weather station "Healy 2 NW" is located near Glitter Gulch, while the "Matanuska" station is located near Long Lake. Note that the local climate varies between the two sites. The two significant climatic factors controlling the hillslope erosional processes are precipitation, and freeze-thaw days. Freeze-thaw days are defined as days in in which the diurnal temperature varies above and below 32 degrees F. As freeze-thaw days are indicative of temperature cycling, erosion would be generally expected to increase with the number of freeze-thaw days. The effects of precipitation

depend upon both the intensity and duration of an individual precipitation event; however, hillslope erosion is generally proportional to the mean annual precipitation.

Table 1 Climatological Data (Western Regional Climate Center)

	Glitter Gulch	**Long Lake**
Dates of Records	1976-2012	1949-2012
Elevation (feet)	149	15
Average Yearly Max Temperature	39.6	44.7
Average Yearly Min Temperature	20.3	26.5
Average Yearly Mean Temperature (F)	29.9	35.6
Annual Days of Max Temp under 32 F (days)	121	96.7
Annual Days of Min Temp under 32 F (days)	212	203
Freeze/Thaw Days (Min – Max under 32F)	91	106.3
Mean Yearly Precipitation (inches)	14.75	15.27
Mean Yearly Total Snowfall (inches)	76.7	47.7
Annual Days with at least .01 inches precip	100	96

Chapter 2 Lidar Data Collection

In 2012, both mobile and static laser scans were collected. The 2012 scans were intended to provide the initial slope characterizations, and the baseline data for later change analysis of time series scans.

The first collect was completed between September 4-14, 2012 by surveyors from David Evans and Associates using their *TITAN*® mobile laser scan system. The vehicle speed during acquisition was typically 25-30 mph, and a minimum of six vehicle passes were required to collect sufficient data coverage and density.

Because some features were difficult to capture from the perspective of the moving vehicle on the highway, supplemental terrestrial static scans were collected using a Leica *ScanStation*. These static collects were made from more advantageous and safer locations off the highway; however, even at these sites, surveyors were unable to collect data for some features, such as the tops of cliffs, or features behind guard rails and other barriers. Additional survey control was necessary to link the mobile and static scans together into a single point cloud.

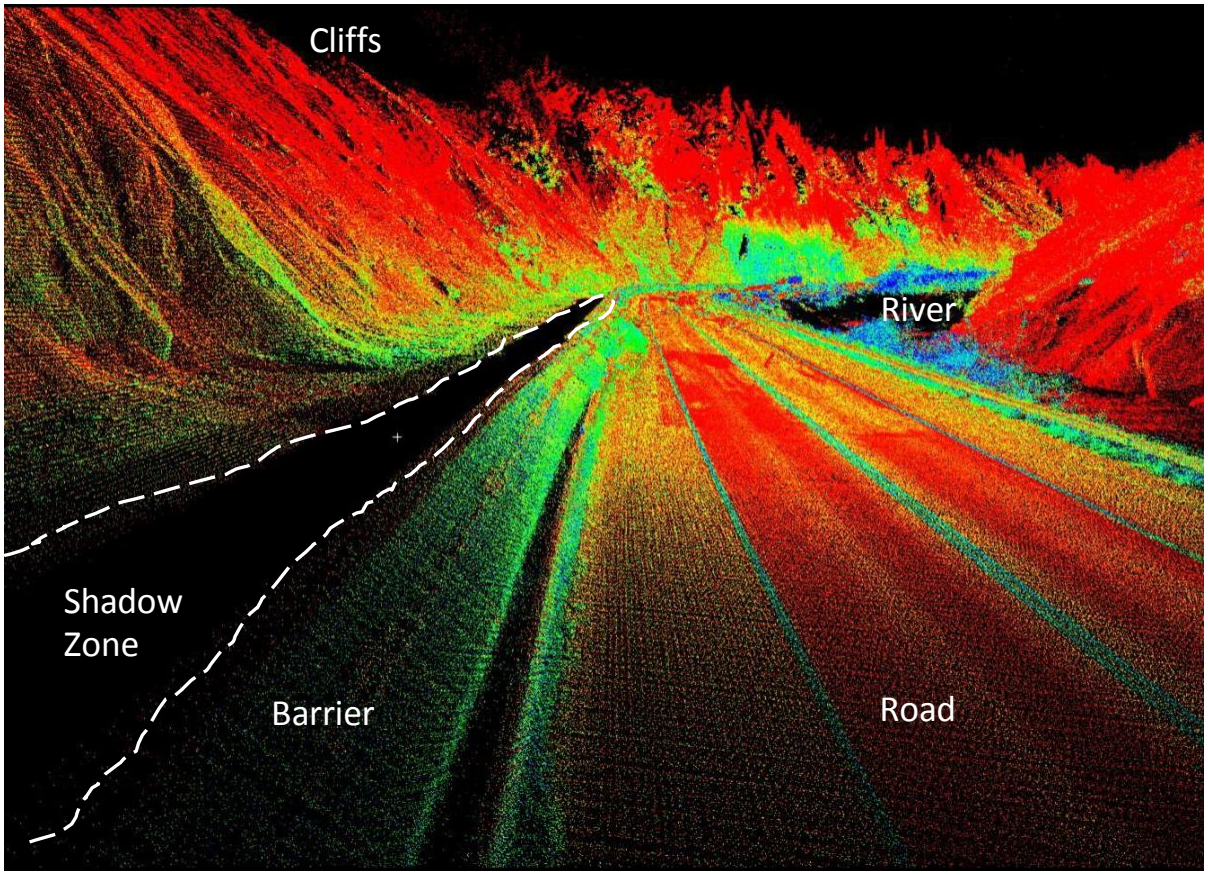

Figure 6 Shadows in point cloud due to mobile lidar perspective

Cameras facing forward and to the side of the vehicle collected video at one frame per second. This imagery was later used to colorize the lidar point cloud. The colorization of the point cloud allows better interpretation of the lidar point cloud including the complex geology of the slope with natural colors for the different rock types and talus.

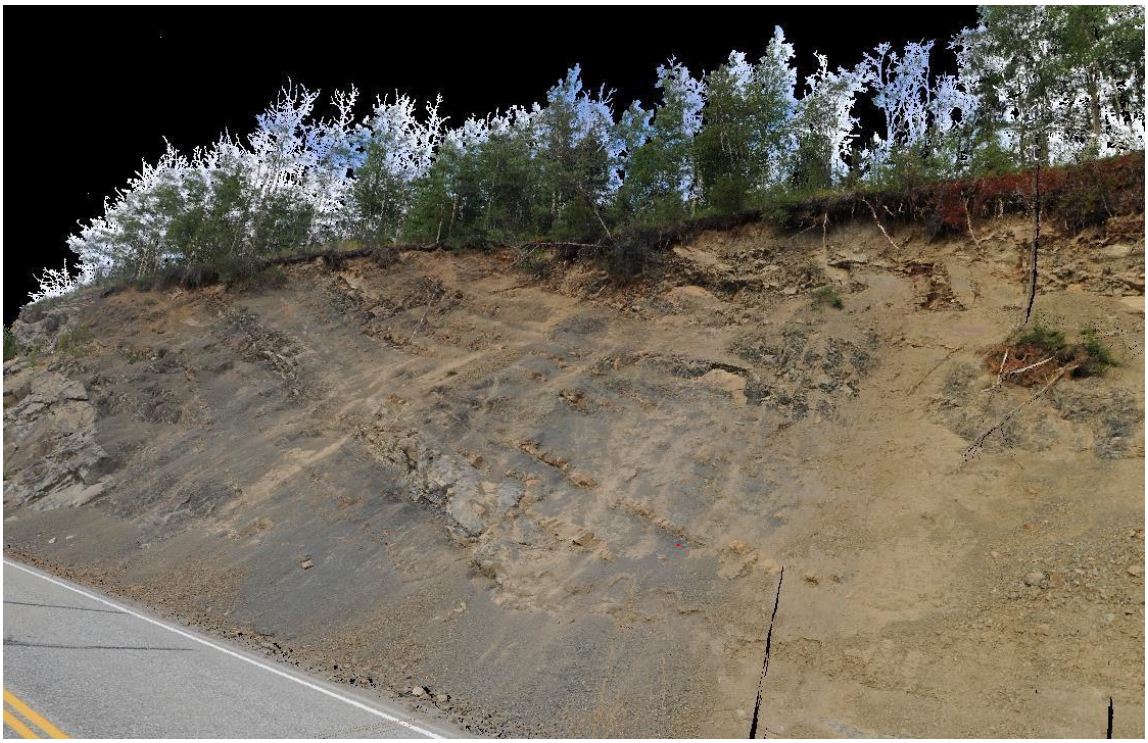

Figure 7 Colorized point cloud of Long Lake geology

Static terrestrial lidar was used for the 2013 collection, and graduate students from Oregon State University (OSU) employed a *Riegl VZ-300* 3D terrestrial laser scanner for a second survey in August 2013. This second survey utilized a "stop and go" approach with the laser scanner. A wagon and tripod mount allowed the lidar scanner to be swapped for a *Trimble R8* GPS receiver and a *Nikon D700* digital camera; this made it possible to calibrate transformation offsets (translations and rotations) for the scanner origin and apply these to the sensor data.

Each scan covered a 360 degree horizontal field of view, with a 100 degree vertical field of view (-30 degrees to +70 degrees from the horizontal plane). Each position was occupied with the GPS for at least 20 minutes to enable a faster static GPS data collection. Six photographs forming a 360-degree view were acquired at each scan position.

Atmospheric conditions (temperature, pressure, and relative humidity) were recorded during the laser scan in order to calibrate data acquisition. Inclination sensors are also included in the scanner to correct for the scanner being out of plumb because of the wagon platform.

Scan positions were typically 50-80 meters apart. Traffic safety and suitable locations for the best scans were considerations that determined the actual distance between scan locations. At Long Lake, 65 scans covering 5.4 km of highway slope were collected. At Glitter Gulch, 76 scans were completed, covering approximately 4.2 km,

The August 2014 collection used the same lidar survey equipment and procedures. Again, this collection was made by graduate students from Oregon State University (OSU). Additional scans were completed adjacent to the slopes in this survey to better capture talus deposits and ditches close to the slopes.

Lidar Pre-Processing Steps

Geo-referencing is a critical step in relating data collected at different time intervals. Since each scan is normally recorded in its own scanner coordinate system, one scan is not relatable to another unless it is transformed into a common systems of units and coordinates. All data were collected and processed in the Alaska State Plane North Zone 4 coordinate system, using the NAD-83 horizontal datum and the NAVD-88 (Geiod12A) vertical datum. The units are meters.

All of the points in the lidar point cloud are then classified according to rules and statistical filters. For this research, we need only to have the lidar returns that create the bare earth model of the soil and rock. However, bare earth may be obscured by vegetation, or by other features, such as passing cars. There are also other types of noise in the lidar data that needs to be removed, including atmospheric noise created by humidity, and spurious reflections of lidar

energy reflected from water surfaces. Our goal for comparing slopes is to filter everything but the bare earth and rock from the data to be compared.

The software used to scrub and classify the lidar point cloud has sophisticated automation utilizing a variety of statistical methods. However, these algorithms require considerable human supervision and assistance to ensure that the algorithms perform correctly. Additional software was developed for this project to assist with processing special morphologic features that characterize the slopes being analyzed – including the curvature of the slopes – and to account for rock overhangs. Finally, manual quality control was performed to remove any remaining lidar artifacts.

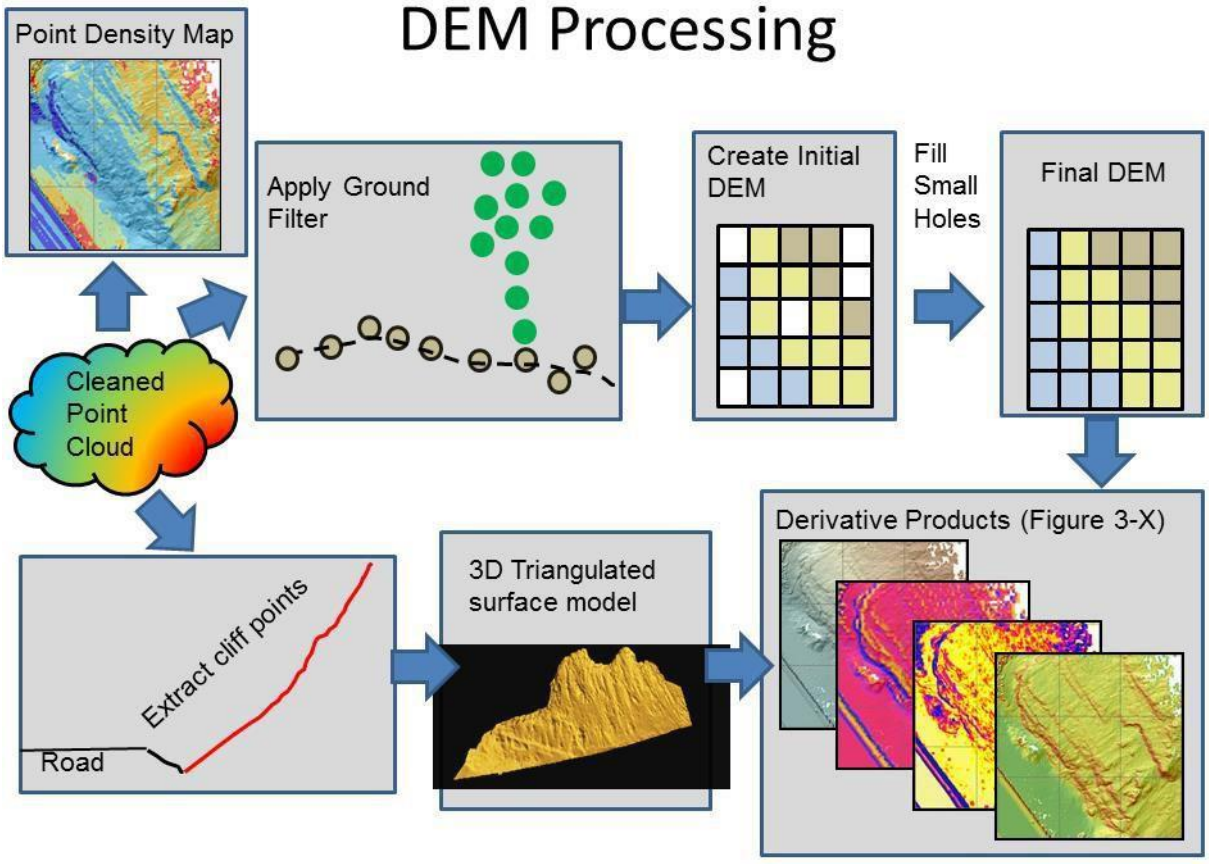

Figure 8 DEM Processing and creation

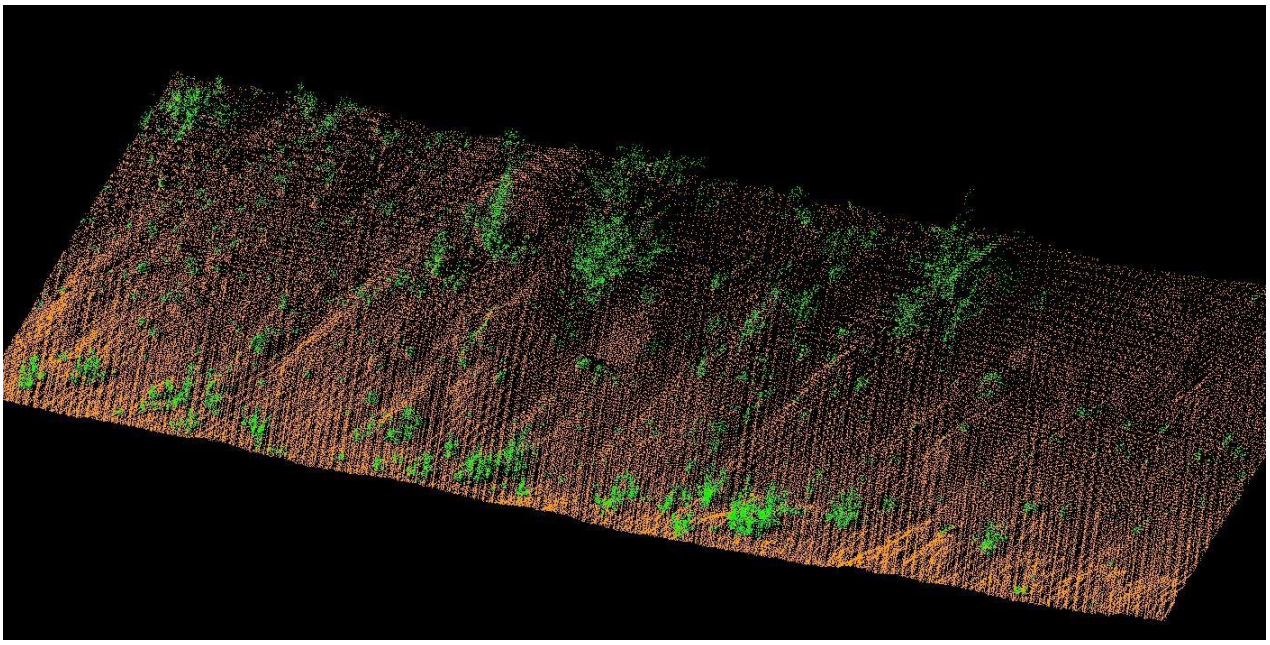

Figure 9 Oblique Ground Filter applied to the 2012 mobile lidar data at Long Lake
Green = classified as vegetation, brown = classified as ground

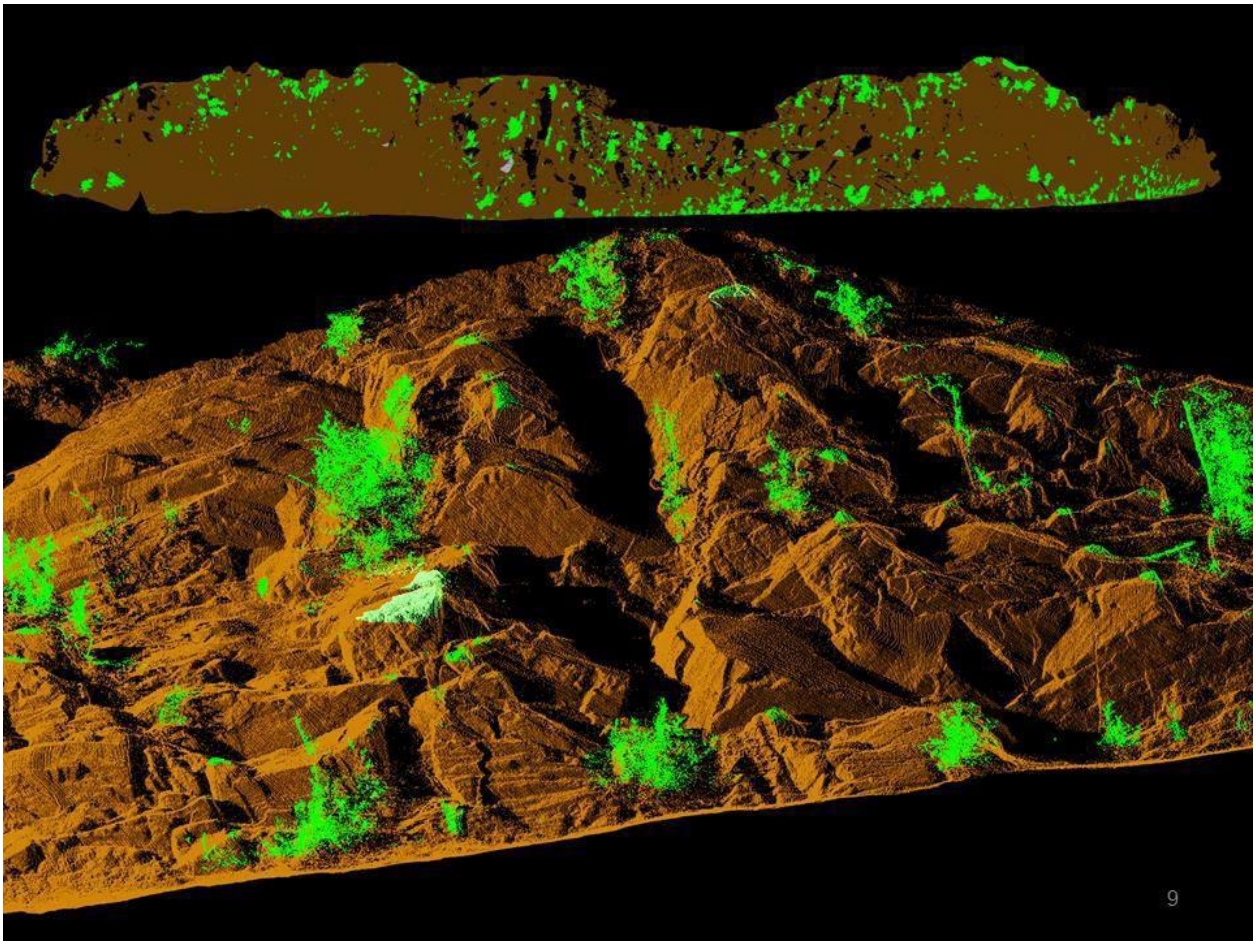

Figure 10 Oblique Ground Filter applied to the 2014 lidar data at Long Lake MP87
Green = classified as vegetation, brown = classified as ground
Top = entire section, bottom = close-up view.

Preliminary Lidar Data Products

Two data extracts generated from the filtered lidar point cloud can be used for analysis and to perform change detection. One is a gridded raster file typically referred to as a digital elevation model (DEM). The other type is the triangulated irregular network (TIN), a type of vector bare earth file created by connecting the lidar return vertices into a mesh of triangles to generate a surface of triangular faces.

The DEM is basically an image like an air photo, with elevation values encoded in each pixel. For visualization, the analyst is limited to very simple color ramps to display elevations. Automated software analysis, including change detection, is only possible with nadir-looking algorithms, where the software assumes the calculations are straight down at the DEM. That form of change detection analysis is not well suited to angled and curving surfaces of slopes along a highway corridor.

The TIN is a surface model that can be viewed from any perspective, even from beneath. This can be an advantage if processing techniques can utilize the perspective of the slope in various calculations; for example, the lidar point cloud can be analyzed from a look angle that is generally orthogonal to the slope. This technique improves the quality of later change detection, but also minimizes issues related to slope curvature and rock overhangs. The TIN also has the advantage of being able to visualize surface roughness better than the DEM, because the surface can be shaded with arbitrary angles of illumination in order to help the human visualize the slope. The Phase I report describes TIN surface modeling in greater detail.

It should be noted that both the DEM and TIN data extracts are commonly described as three-dimensional. However, this is a flawed definition because there is no data beneath the surfaces of the DEM or TIN. A more accurate description of the surface models is two-and-a-half dimension (2.5D), as it does contain elevation data not found in a 2D model, but it is not a complete 3D representation.

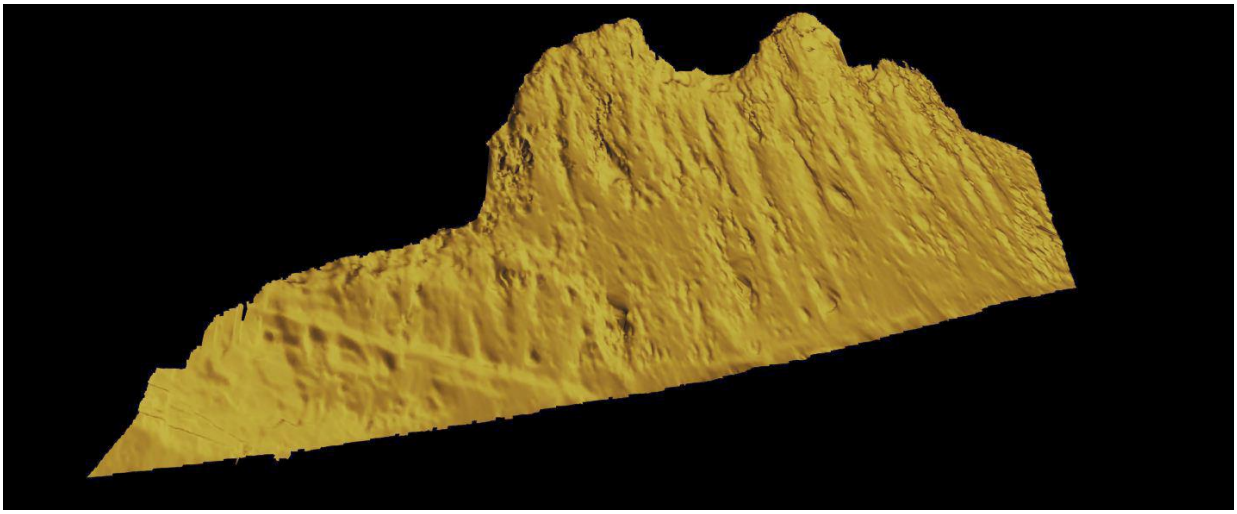

Figure 11 Example of a triangulated surface mesh at the Long Lake site

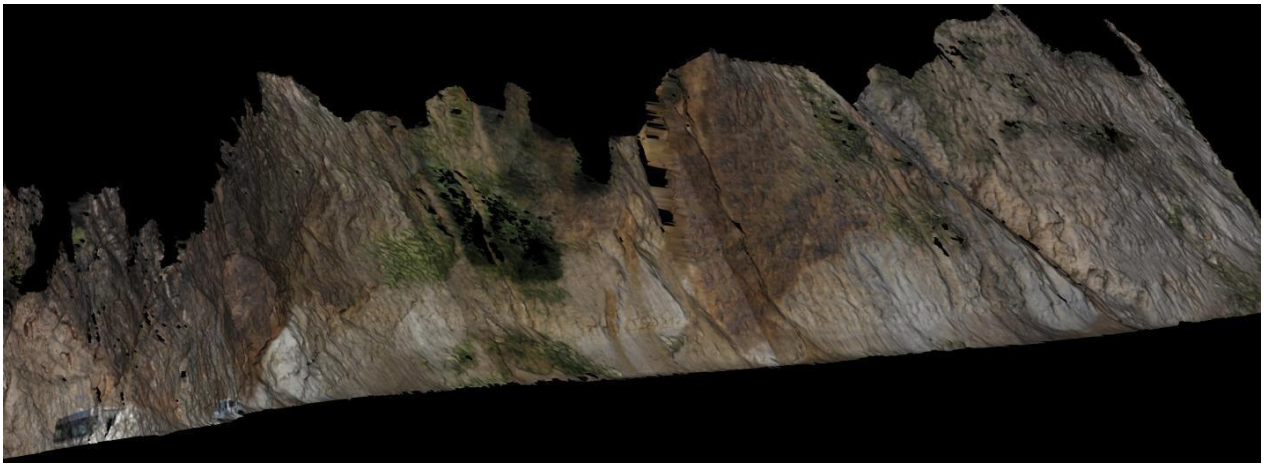

Figure 12 Example of a colorized triangulated surface mesh at the Glitter Gulch site

A variety of derivative products were developed from these TINS to improve analysis. These products were created with a grid that was set to the best fit plane to the cliff rather than in the XY plane for improved classification results and modeling of overhangs. Figure X below shows an example of the types of products that can be produced from the 2.5D TIN model. The key steps in generating these models are

1. Importing the lidar dataset that has been cropped to the area of interest for a section of cliff

2. Determining the spatial extents of the dataset and centroid
3. Calculating the best fit plane for the data points
4. Rotating the data about its centroid so that the best fit plane aligns with the XY axis
5. Dividing the dataset into cells (e.g., 50 cm)
6. Determining the minimum point per bin to create a course ground model
7. Creating a smoothed grid using a focal operator (comparisons of neighboring cells) to determine the median values of cells within a window
8. Filtering out points too far above and below a threshold distance above the smoothed grid created in 7
9. Repeating steps 5-8 with incrementally smaller cell sizes (e.g., until the cell size is 5cm) using only the ground classified points
10. Once the iteration is complete, calculating the centroid of all ground points in each grid cell
11. Formulating triangles between neighboring centroids in each grid cell using the methodology of Olsen et al. (2013).
12. Rotating the dataset back to its original coordinates (inverse transform of step 4).
13. Calculating the surface normal (normalized to a unit vector) for each cell based on the connectivity of its centroid with neighbors
14. Calculating the 3D slope for each cell from its surface normal
15. Obtaining several surface roughness values by determining the standard deviation of slope within a variety of window sizes centered on the pixel of interest (e.g,, 7x7 cells, 17x17 cells).

16. Perform clustering analysis using a connected components algorithm to identify clusters of positive and clusters of negative change for individual failure analysis.

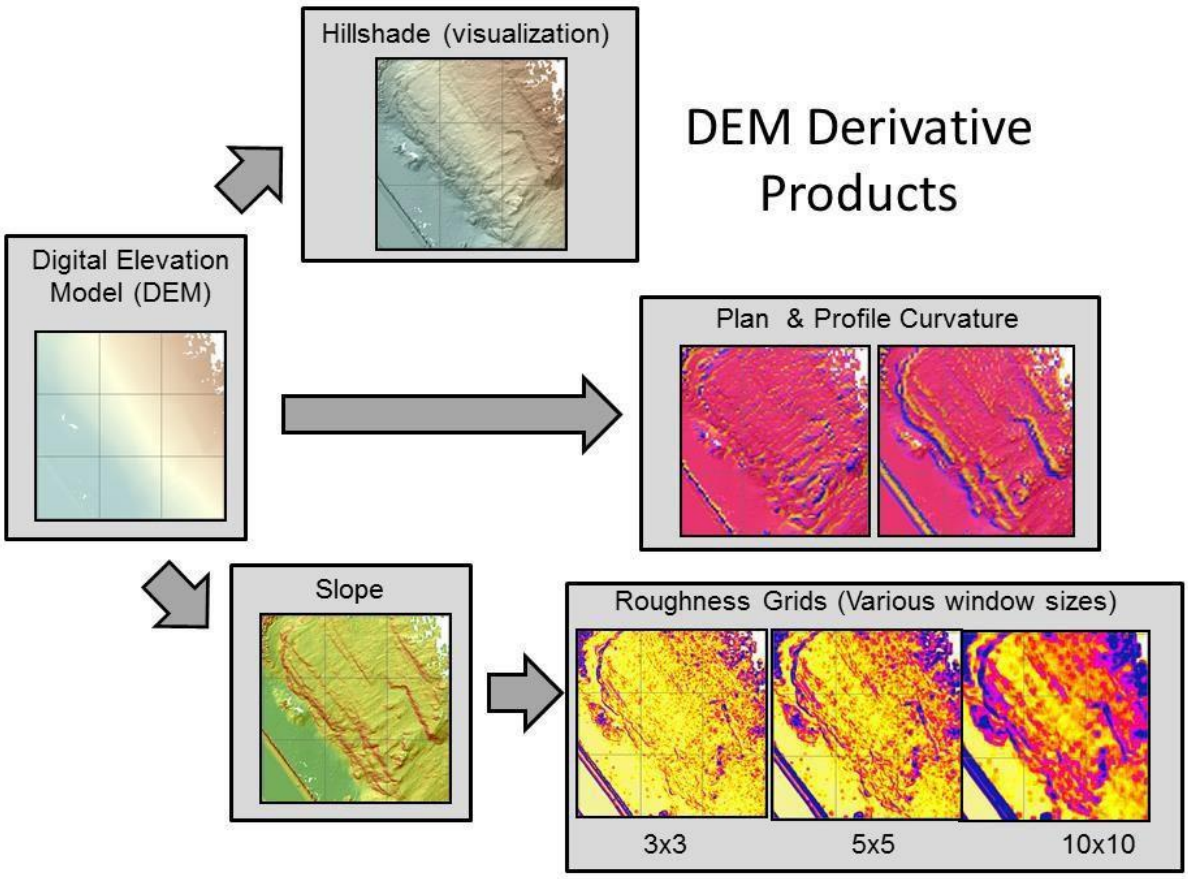

Figure 13 DEM Processing Steps and Products

Geo-referencing Accuracy Evaluation

To ensure that the change detection methods are accurate, a rigorous quality control process was implemented. For this slope study, significant time was spent to ensure that any detected change is accurate. One component of the quality assurance process is comparing the lidar point cloud to another set of survey data. The accuracy comparisons were typically in the

range of 3-4 cm (3D RMS) at both the Long Lake and Glitter Gulch project sites; however, in some cases, poor GPS quality resulted in degraded accuracies of 7-8 cm (3D RMS).

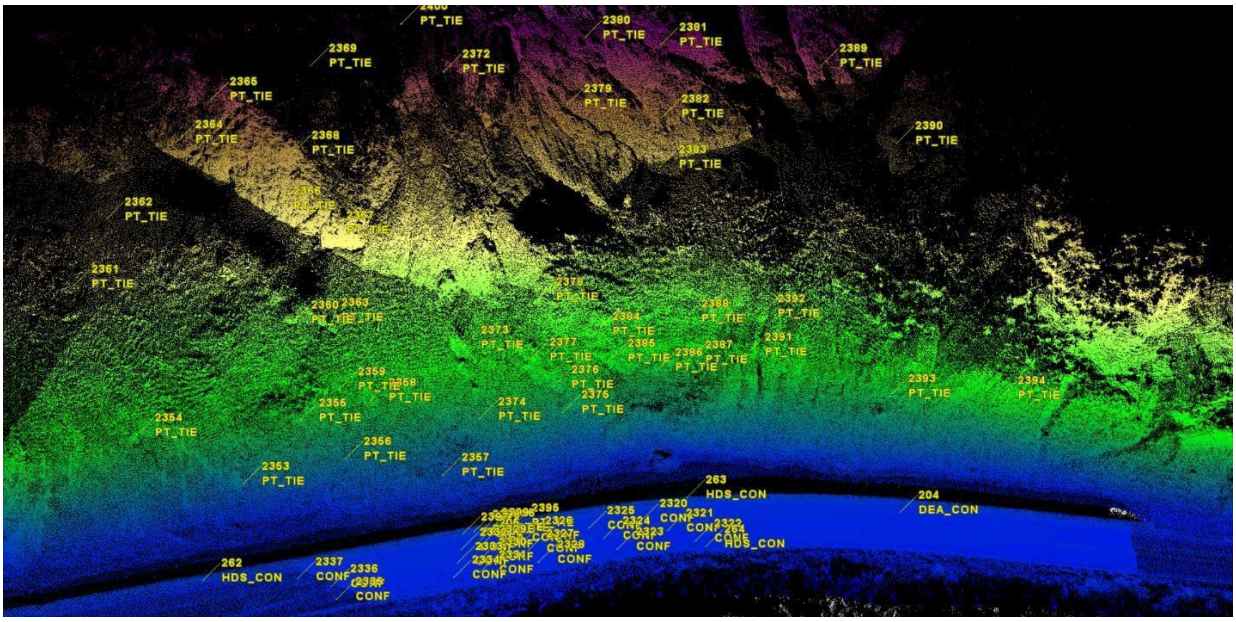

Figure 14 Example of validation points collected with a total station

Table 2 Summary statistics of validated elevation data (in meters)

Δz (m)	Long Lake	Glitter Gulch
Average	-0.003	-0.008
Minimum	-0.179	-0.087
Maximum	0.093	0.067
Average (absolute)	0.020	0.025
RMS	0.035	0.031
Std. Dev	0.035	0.030
95% confidence	**0.069**	**0.061**
# validation points	169	124

Chapter 3 Change Analyses

The data collected in 2013 and 2014 can be compared using baseline lidar data from 2012. The comparison subtracts the baseline from the time frame being studied, and differencing the two lidar files can then be used to create a new set of lidar data that shows the change. This change detection technique allows the user to analyze the erosion and accretion of the slope. The analysis, coupled with the colored lidar data generated from the digital imagery, also permits the consideration of how specific geologic features are factors in the slope's change.

The first step in the change analysis process is the precise co-registration of the lidar bare earth files being compared. Even with accurate geo-referencing of the point cloud with GPS coordinates, there are small errors or differences in the GPS that result in the data being compared to not match as they should. The co-registration is accomplished by identifying points in common between the lidar data sets that have not changed. These registration points can be pre-marked targets placed during the lidar collect, or matching points in the point cloud. Any biases in the data are removed by shifting one lidar point cloud to match the registration points in the other data set. Removing the bias is done with a least squares, rigid-body coordinate transformation, that applies both a rotation and translation along orthogonal axes, which results in the minimization of the sum of the square errors between point pairs. With the two co-registered lidar bare earth models, the difference in the two can be calculated.

Two software applications were used for change detection, each with their own advantages and disadvantages: *CloudCompare* (v101.99), an open source program; and *Maptek I-Site Studio* (v4.2), a commercial solution. In general, our observations were that the *Maptek I-Site* seems to have a more reliable change detection algorithm, while *CloudCompare* has superior

visualization options. By using both programs, we were able to validate the change detected and quantified.

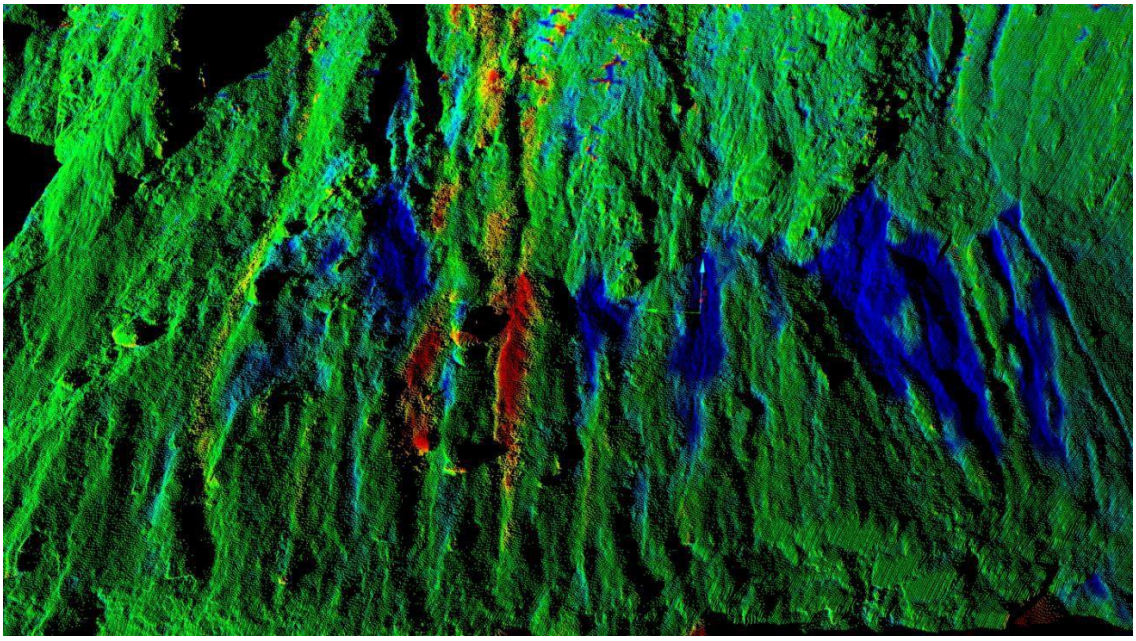

Figure 15 Close-up of eroded material (blue < -0.25m) at Glitter Gulch.

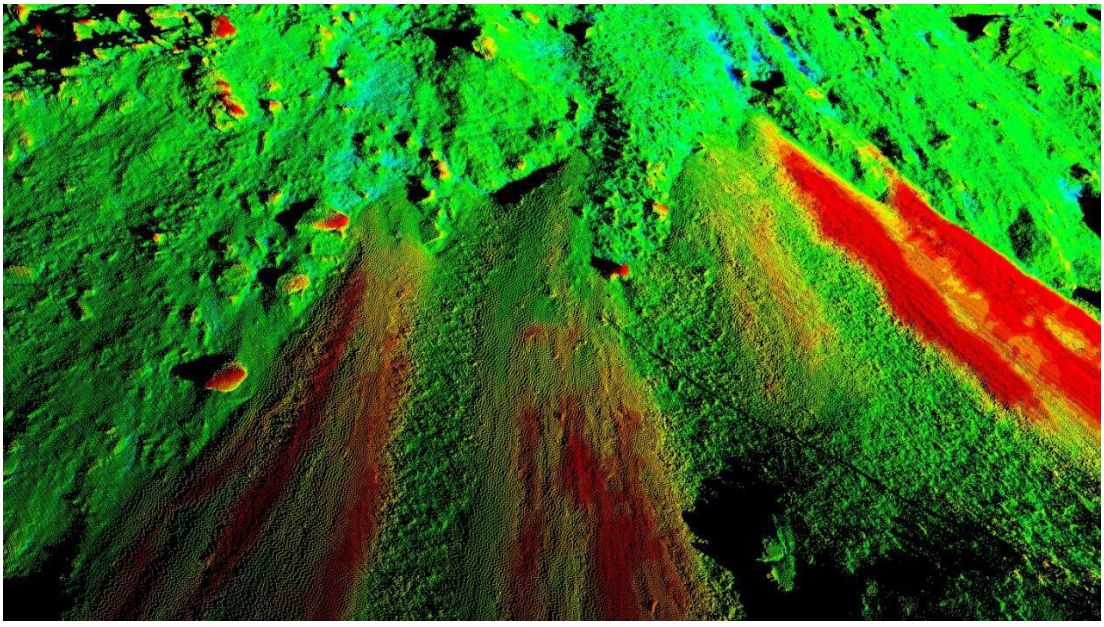

Figure 16 Close-up of accreted material (red > 0.25m) and eroded material (blue < -0.25m) at the Glitter Gulch.

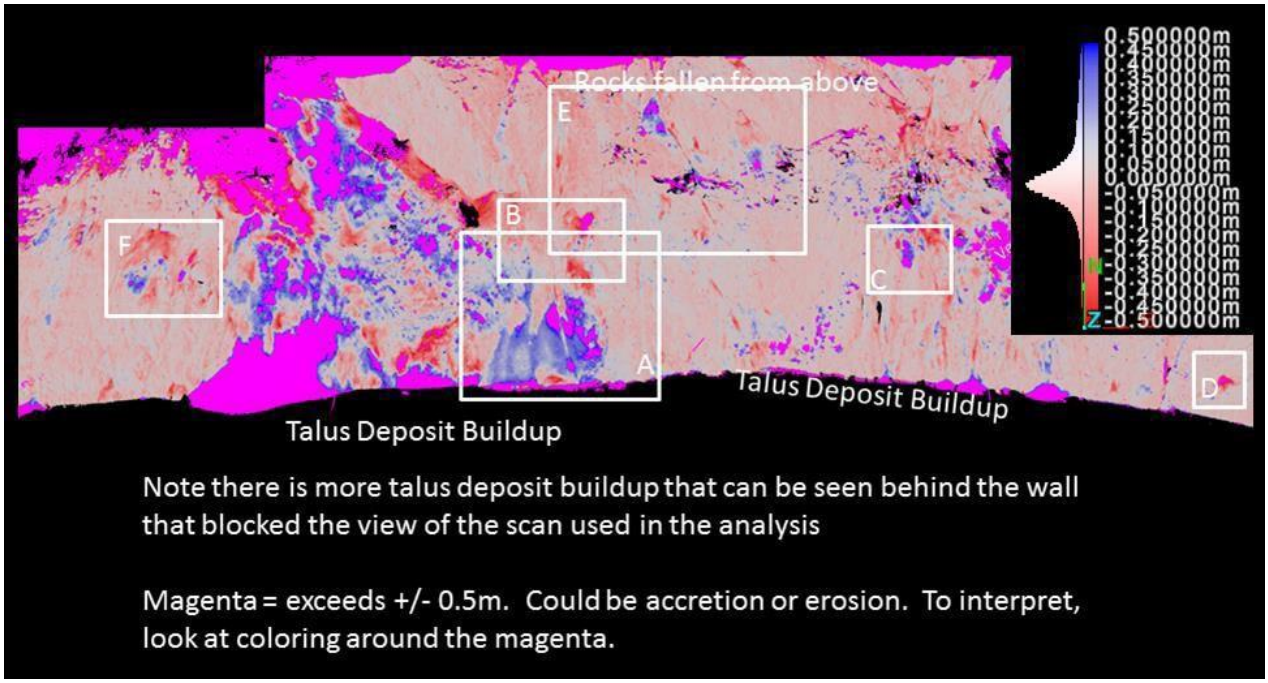

Figure 17 Change analysis at Glitter Gulch (See Figure 19 for subsets)

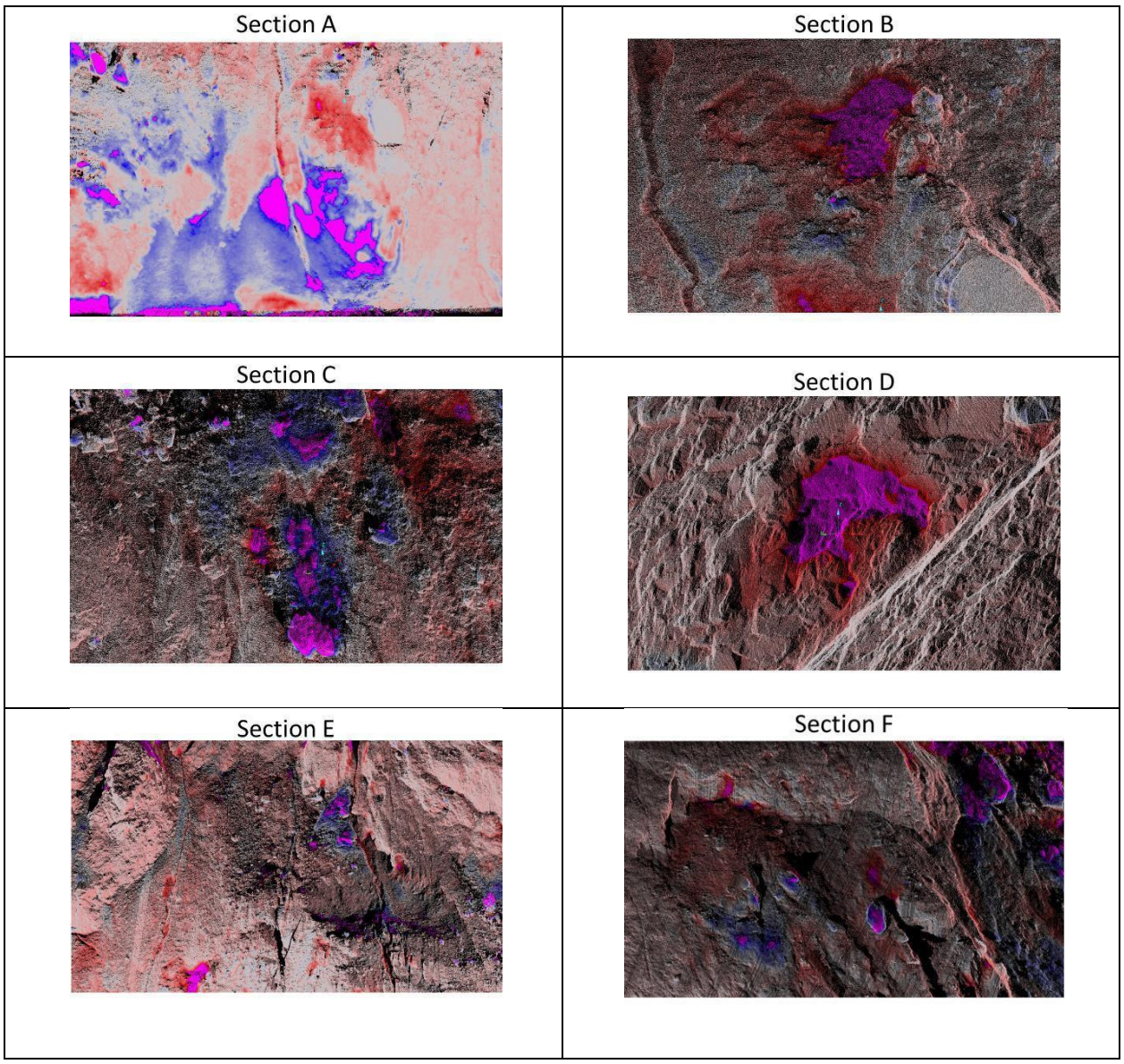

Figure 18 Detailed analysis of six sections at Glitter Gulch

Chapter 4: Novel Lidar-Based Slope Assessment System

Rock-slopes along transportation corridors evolve in response to the structural characteristics of the rock mass and natural weathering processes. Rock-slope classification and assessment systems have traditionally focused on only one of these two aspects of rock-slope evolution. For example, the popular Rockfall Hazard Rating System (RHRS; Pierson, 1991) captures the structural features of rock masses (e.g. discontinuity spacing and patterns; location of rock overhangs, dip of discontinuities, block size). Alternatively, the Rock-slope Deterioration Assessment system (RDA; Nicholson, 2005) focuses on the weathering characteristics of rock masses (e.g., rock strength, weathering grade, fracture aperture, and fracture spacing). Both types of assessment procedures rely on manual field-based assessment of rock slope parameters.

New technologies such as lidar allow high resolution topographic and morphological data to be collected in rapid, cost-effective manner. We are now finding that our data collection and analysis abilities have begun to outpace the available rock-slope classification tools.

In this chapter, we describe a new lidar-based rock-slope assessment system that captures both rock mass structure as well as weathering/erosion processes. In this approach, termed the Rockfall Activity Index (RAI), topographic and morphologic change is used to quantify rock-slope activity and assess the relative rock-slope failure hazards

The Rockfall Activity Index (RAI)

Rockslope Activity Index (RAI) is a lidar-derived assessment system that considers both rock structure and its weathering. Through this system, rock slopes can automatically be classified into different morphological categories which are then evaluated for hazard. Rock slopes are assessed for potential hazard by calculating the probability of the kinetic energy released. Sites can be assessed against each other or can be split into sections and assessed

throughout to find areas that are at a higher probability of energy release. This system aims to identify the major slope failure areas

The RAI involves three principal steps:

1. Lidar acquisition and processing
2. Rockslope process analysis
3. RAI hazard quantification

Step 1 is addressed in chapter 2 of this report. Step 2 consists of a classification of the rock-slope using roughness and slope. Step 3 uses the classification coupled with slope height to derive a hazard quantification.

Rockslope Process Analysis

Understanding and characterizing rock slope processes is the first step for quantifying potential hazards. Different processes will have different failure potential as well as different consequences when failure occurs. Some processes are easy to distinguish from others (e.g., collapses of overhangs), while others require more effort to observe and quantify (e.g., raveling slopes). To apply this process across a large area and to utilize dense datasets such as lidar efficiently, each class needs to be characterized.

For RAI, morphological indices were used to distinguish between the classes of processes. The following indices were developed based on a 5cm cell size:

- Slope – The slope, in degrees, calculated from the 3D normal vector for each cell, Hence, these values range from 0 degrees (flat) to 90 degrees (vertical) to 180 degrees (overhang)
- R35 – Roughness 35cm, which is quantified as the standard deviation of slope within a 35 x 35 cm window of cells (e.g. 7 cells x 7 cells), and

- R85 – Roughness 85cm, which is quantified as the standard deviation of slope within a larger 85 x 85 cm window of cells (e.g. 17 cells x 17 cells).

Rock-slope classification for point-cloud derived grid cells are determined based on the logic tree algorithm shown in figure 19, the class of each cell of the grid can be determined through a process of elimination resulting in 7 categories described in table 3. Figure 20 are simple cross sections depicting two different classes of rock overhangs. Figure 21 shows the difference between the 10 cm, 20 cm and 30 cm classes. These sizes are approximate and there is some overlap between these. Generally these classes represent the size of rock which will fail from these areas. Smaller rocks may be large enough to do damage to vehicles when run over such as cracking windshields or oil pans. The 30 cm classification is more indicative of rock failures that might be such that a vehicle would have to swerve to miss. Table 4 shows talus and intact. These two classes are difficult to fully distinguish between with the morphological indices but act similarly in that they are most likely not the trigger points for failure but areas surrounding them such as overhang are more likely to fail such that they too will fail. Another strong distinguishing point between intact and talus is that talus normally does not occur above a soils angle of repose, so areas with smaller angles are more likely to be talus.

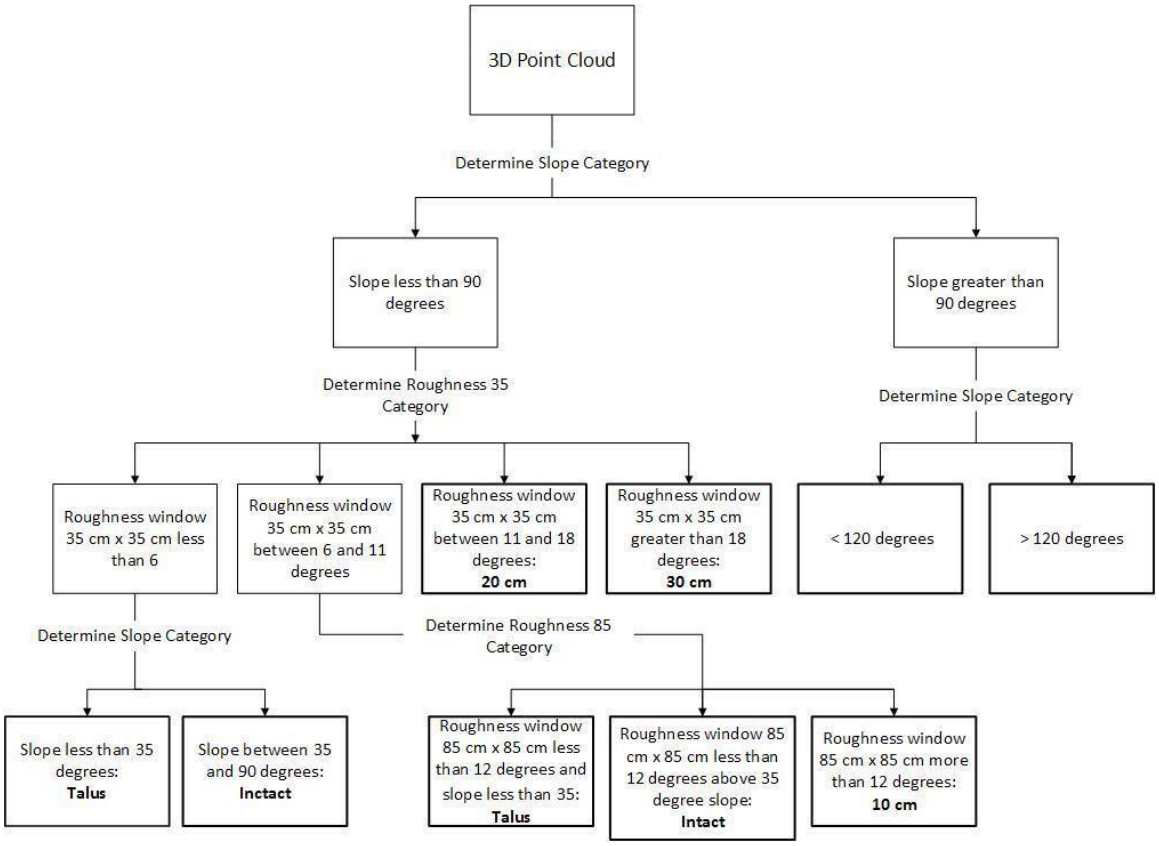

Figure 19 Flow chart of the RAI system. Starting with the 3D point cloud, the slope is first considered so that overhangs can be immediately categorized. After slope, roughness at a small window size (35cm x 35 cm) 30 cm and 20 cm. The last three classifications are determined in part by slope and part by large roughness with a larger window size of 85 cm x 85 cm.

Table 3 Classification names and descriptions

Name	Description
Talus	Small debris mostly found in the bottom of the slope, although can be found throughout the slope
Intact	Little to no fracturing of rock, would act as one large rock if released
10 cm	Rock that is either in place or has moved that is smaller than 10 cm
20 cm	Rock that is either in place or has moved that is between 10 cm and 20 cm
30 cm	Rock that is either in place or has moved that is larger than 30 cm
Overhang <120°	Overhangs from near vertical to 120°
Overhang>120°	Overhangs greater than 120°

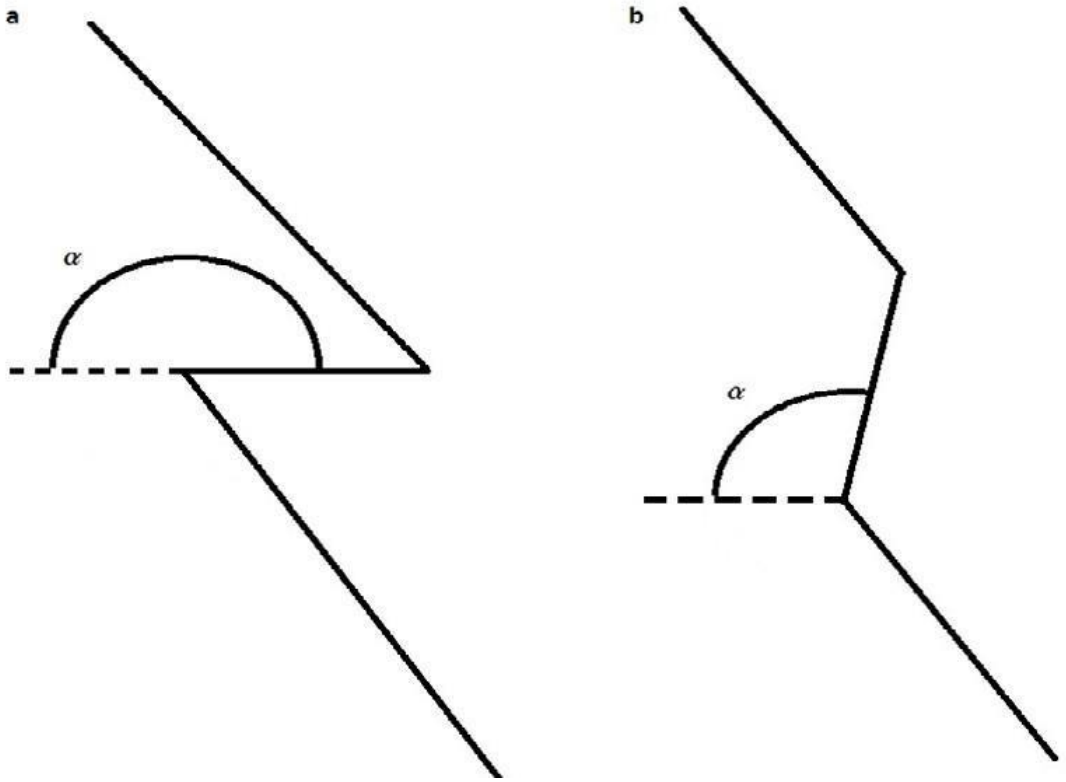

Figure 20 Representation of the difference between overhang > 120 degrees (a) and overhang < 120 degrees (b). Alpha is the angle which is measured for the slope. Larger slopes indicate that more material is above them if failure were to occur, therefore they are considered more hazardous.

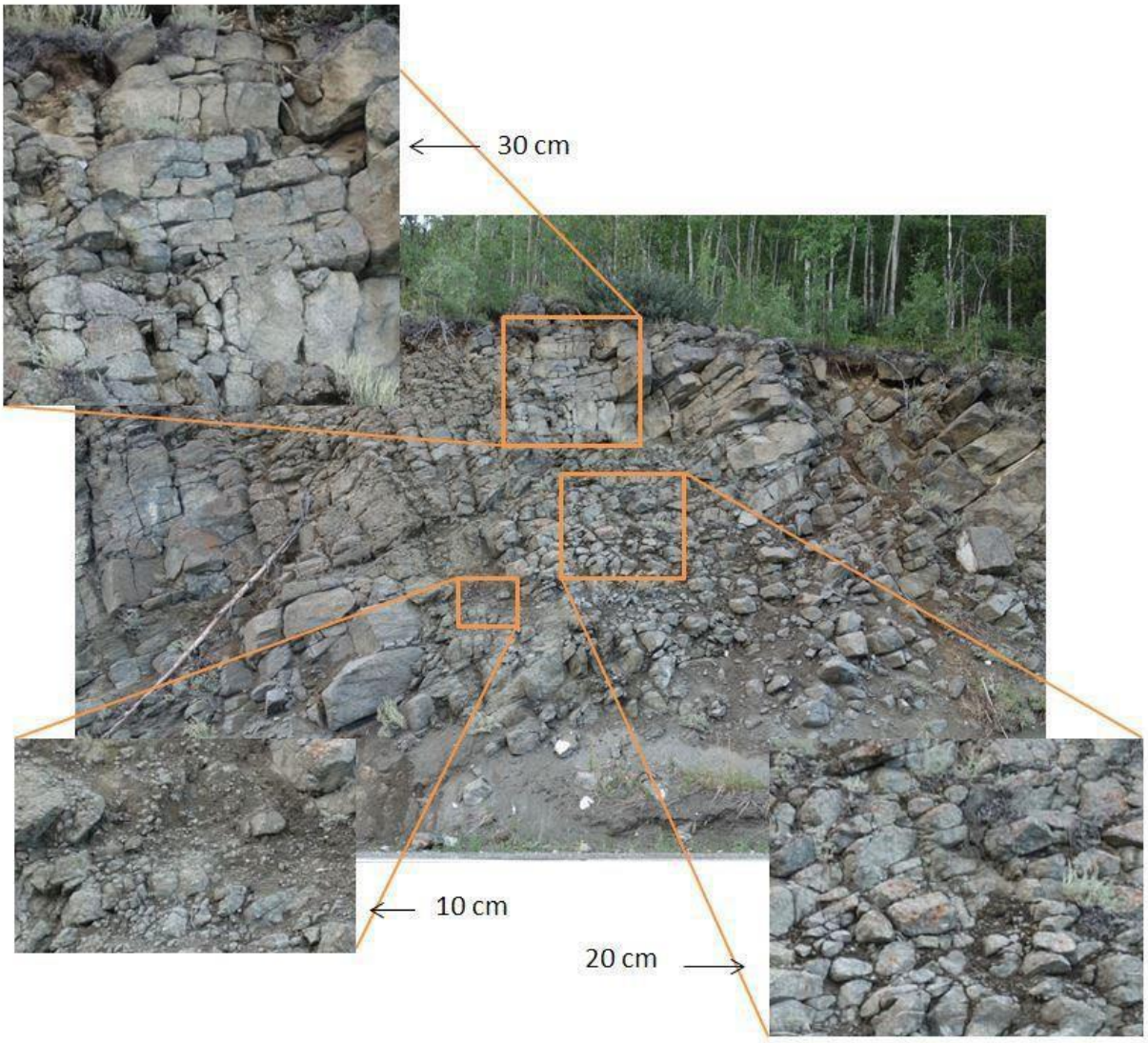

Figure 21 Examples of 10, 20 and 30 cm size categories. These categories are approximate sizes.

Hazard Rating

Once a cell is classified, a hazard rating is assigned based on a Kinetic Energy (KE) release rate or a "RAI" score:

$$RAI = KE * F$$

Here RAI is the rate of KE release to the road surface, and F is the failure rate which is based on change detection. KE is represented by the equation:

$$KE = \frac{1}{2} * m * v^2$$

Where m is mass and v is velocity. Estimates of mass and velocity, are established through assumptions about the classes and using the height of each cell from the road surface. Therefore, there are three factors to be calculated as inputs into the RAI score, mass, velocity and probability of failure. Each of these will be discussed in more detail.

Mass

Mass is estimated by calculating the assumed volume of a potential failure that varies with RAI class. In adopting an assumed volume, the average length and height were taken from the 3D point cloud for each class. The results are summarized in Table 2. For the overhangs, it was assumed that if they were to fail, a portion of the rock mass above would also fail. Thus the average height of an overhang was calculated including areas of intact rock which might fail above it. Because of distortion caused in the grid, the length was assumed to be 7.5 cm for overhangs less than 120 degrees and 10 cm for those above instead of the 5cm assumed for other classes.

Table 4 Measurements for calculating the cube size and cube size

RAI class	Length (cm)	Height (cm)	Width (cm)	Cube Size (cm^3)
Talus	<1	<1	<1	<1
Intact	5	>100	5	>2500
10 cm	5	8.1	5	203
20 cm	5	18.4	5	460
30 cm	5	39.9	5	998
Overhang < 120	7.5	78.4	5	2941
Overhang > 120	10	78.4	5	3921

Mass

With the cube size as volume, the mass can be calculated for each cell assuming a uniform specific gravity:

$$m = V * ??$$

Where m is mass, V is volume or cube size and SG is specific gravity, which is assumed to be 2.7.

Velocity

To calculate volume the height was used. Velocity can be estimated from the terminal velocity equation:

$$v = \sqrt{2 * g * h}$$

Where v is velocity, g is the acceleration due to gravity (9.807 m/s^2) and h is the vertical distance between the road surface and cell in meters.

Failure Rate

The change detection from two consecutive years of co-registered scans was used to determine failure rate. This calculation was normalized by the total number of cells in each class giving a normalized failure rate for each class which, can be seen in Table 5.

Table 5 Typical failure rates in each of the RAI categories over a 1-year period

RAI Classification	Failure Size (cm^3)	Failure Rate
Talus	1	0.000001
Intact	125	0.000001
10 cm	201.4	0.000413
20 cm	459.7	0.000666
30 cm	997.2	0.001129
Overhang <120	2760	0.000674
Overhang >120	3680	0.001867

RAI Implementation

The two test sections along Parks Highway and Glenn Highway have been scanned with high resolution terrestrial based lidar for two consecutive years. The "Long Lake" test site, on the Glenn Highway (Alaska Route 1), included eight sites and Parks Highway test site included five locations. Three sites along the Glenn highway were used for the calibration and development of this system. The locations selected are at milepost 85.0, 85.5, and 87.0. Figure 1 in Chapter 1 shows the location of all sites and labels the selected sites.

Milepost (MP) 87 of Glenn highway is presented here as an example site to illustrate the implementation and results. This site captures many of the morphological features that drive the evolution of slopes. In MP 87, there are several areas of overhang both small and large. Figure 5

shows a close up of one section showing a) a photograph of the area, b) the RAI classification and c) the RAI hazard rating. From a 2D perspective of a photograph, overhangs can be difficult to distinguish. However, the classification system readily highlights overhang areas highlighting them in red and yellow coloring. Areas in blue are those in the 10 cm, 20 cm and 30 cm classifications, while the purple and green are talus and intact, respectively. The hazard map (c) also highlights the overhangs because of the greater potential for failure. Another aspect that affects the hazard rate is the height (h) of slope from the road; as height (h) increases up, the hazard also grows.

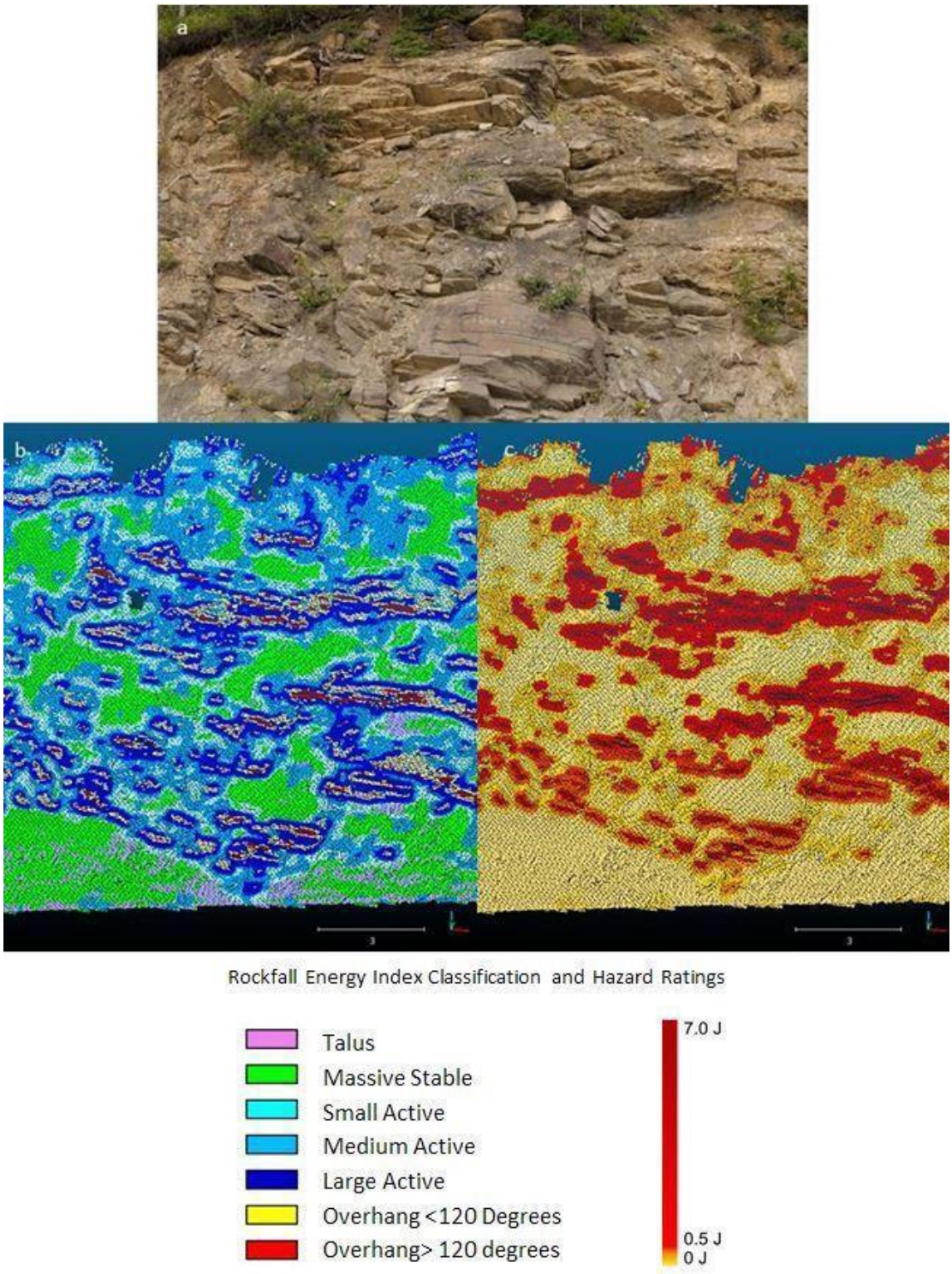

Figure 22 RAI examples: a) photo of the area shown in b) RAI classification and c) RAI hazard rating, that shows the highlighting of overhangs within a system.

The next figure shows the classification of all the sites along Parks Highway and Glenn Highway. The areas along Glenn highway, with the exception of one have lower energy release than those of Parks Highway. Parks Highway geology is of a weaker schist compared to Glenn Highway geology of sedimentary rocks which might partially drive this difference. Other drivers might be the maximum heights at a site or the length of the site. The latter will be addressed in a later section.

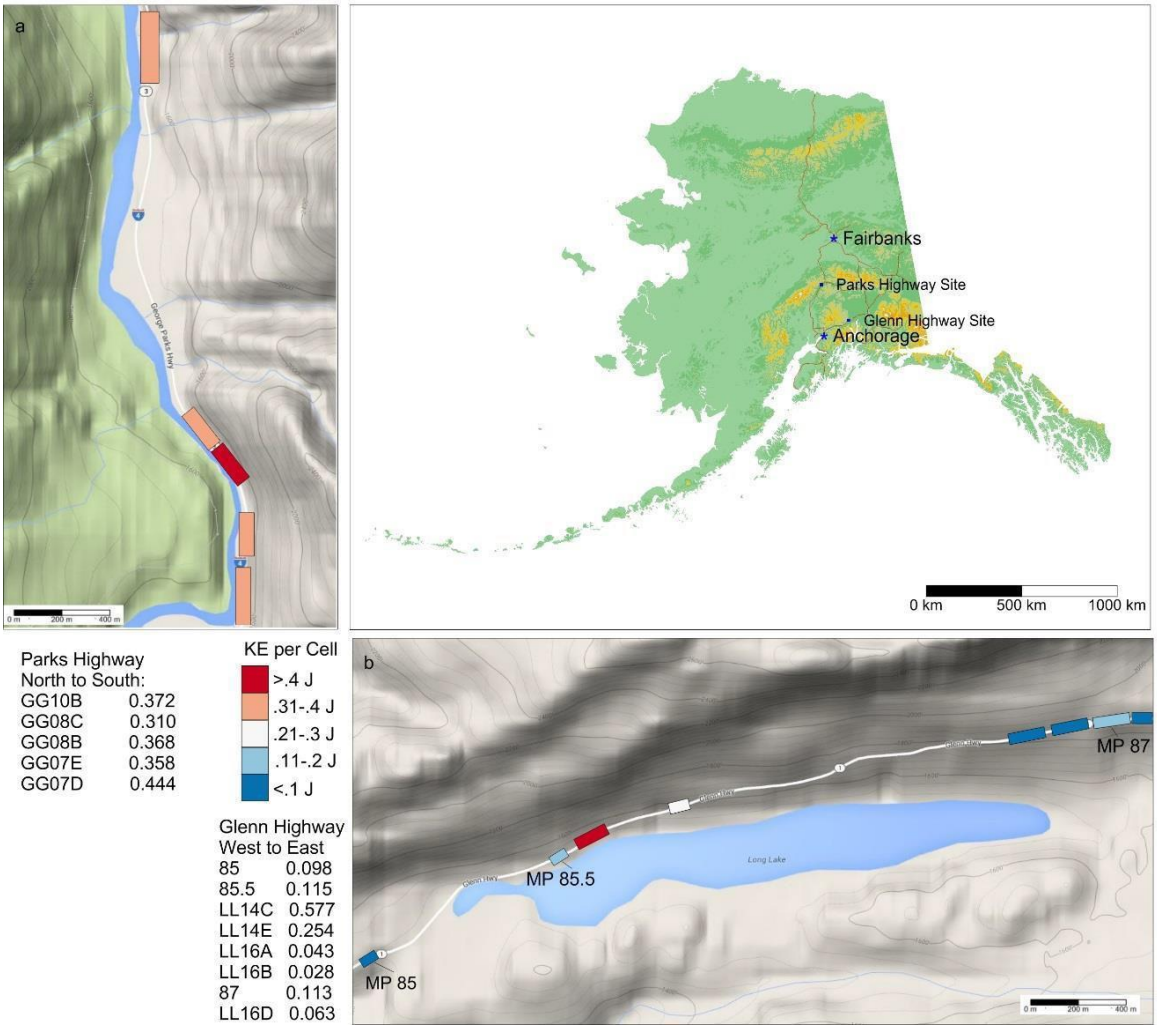

Figure 23 Map of the study areas their RAI scores, a) Parks Highway and b) Glenn Highway

Rockfall Activity Index (RAI) Performance

Figure 24 show an example of the RAI for MP 87 of Glenn highway. The figure shows (a)) the lidar point cloud data, (b) classification system and (c) and hazard rating. Similar data for other sites are included in the Appendix. Visually comparing the RAI with the photographs suggests that the RAI preforms well for classifying the rock-slopes. It is difficult for the RAI to identify individual rock sizes correctly, so the categories of 10cm, 20 cm and 30 cm should be regarded as a generalization of what is occurring within an individual area. For example, a large rock will act more like an intact area towards its center, so the edges of the large rock are picked out, and the center is classified as if less erosion is taking place.

To test the accuracy of the model, *RocFall* 5.0 (Rocscience Inc. 2013) was used to simulate a free fall object. Points on the RAI point cloud were randomly chosen so that there was a sample containing all the types of classes. Each point was queried for the RAI classification, RAI hazard score and height from the base. In *RocFall* a rock the size of the class was dropped from the height and the total kinetic energy was recorded. For normalization purposes, each *RocFall* calculation was divided by the RAI hazard score. Table 6 shows the results according to class and height from the bottom of slope. The RAI is conservative compared to the *RocFall* model, calculating a higher energy release. The level of conservatism depends upon the class and the height from the bottom of the slope.

Table 6 Comparison between rockfall analysis and RAI for different classes and slope positions

RAI Class	Percent RAI	Height less than	Percent RAI
small	99.3	**2.5m**	3.6
medium	66.5	**5m**	17.9
large	35.1	**7.5m**	28
<120	18.4	**10m**	58.1
>120	51	**10m+**	57.6

In the next three figure, the overall score for each site was shown, but each site can be divided into smaller geographic segments for a more generalized quantitative analysis of the risk along the highway. Figure 9a represents the cumulative RAI score across 10-meter road-length segments for MP 87. These generalized RAI assessments allows one to identify the sites which present the highest risk and find what portions of the slope are contributing to that risk.

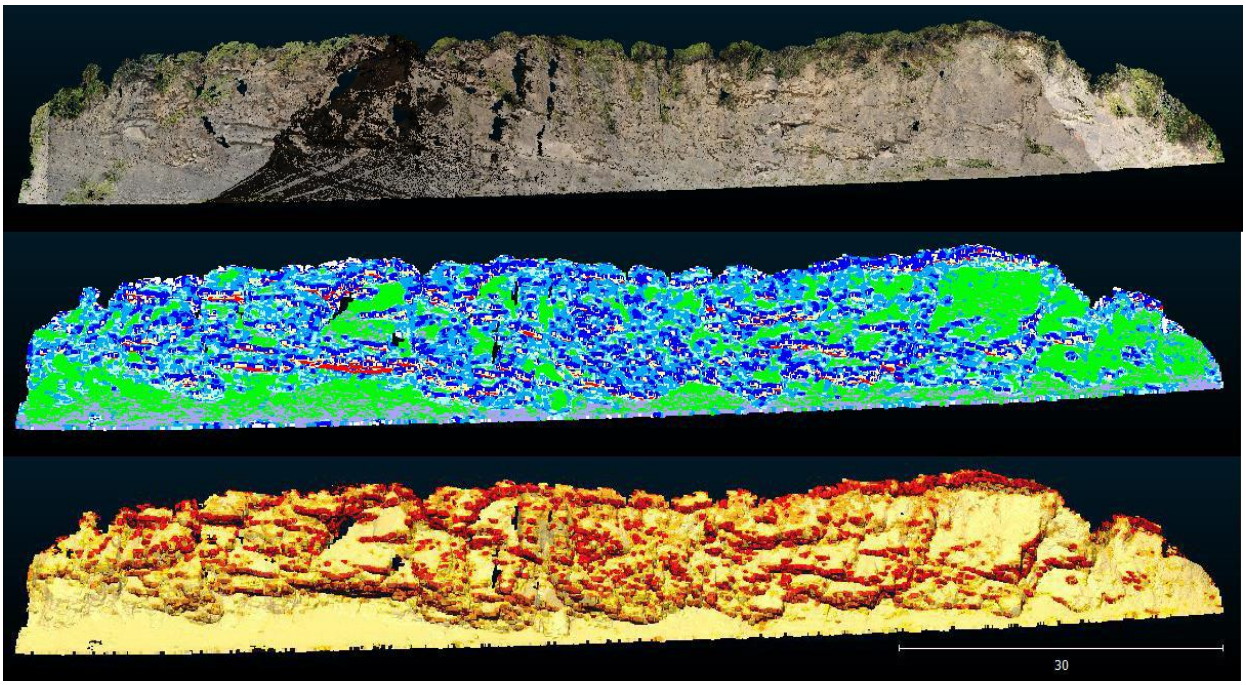

Figure 24 MP 87 of Glenn Highway: a) lidar point cloud data, b) RAI classified cloud and c) RAI hazard rating. Note the small black sections are areas where there are holes in the coverage due to shadow and lidar scanner positions.

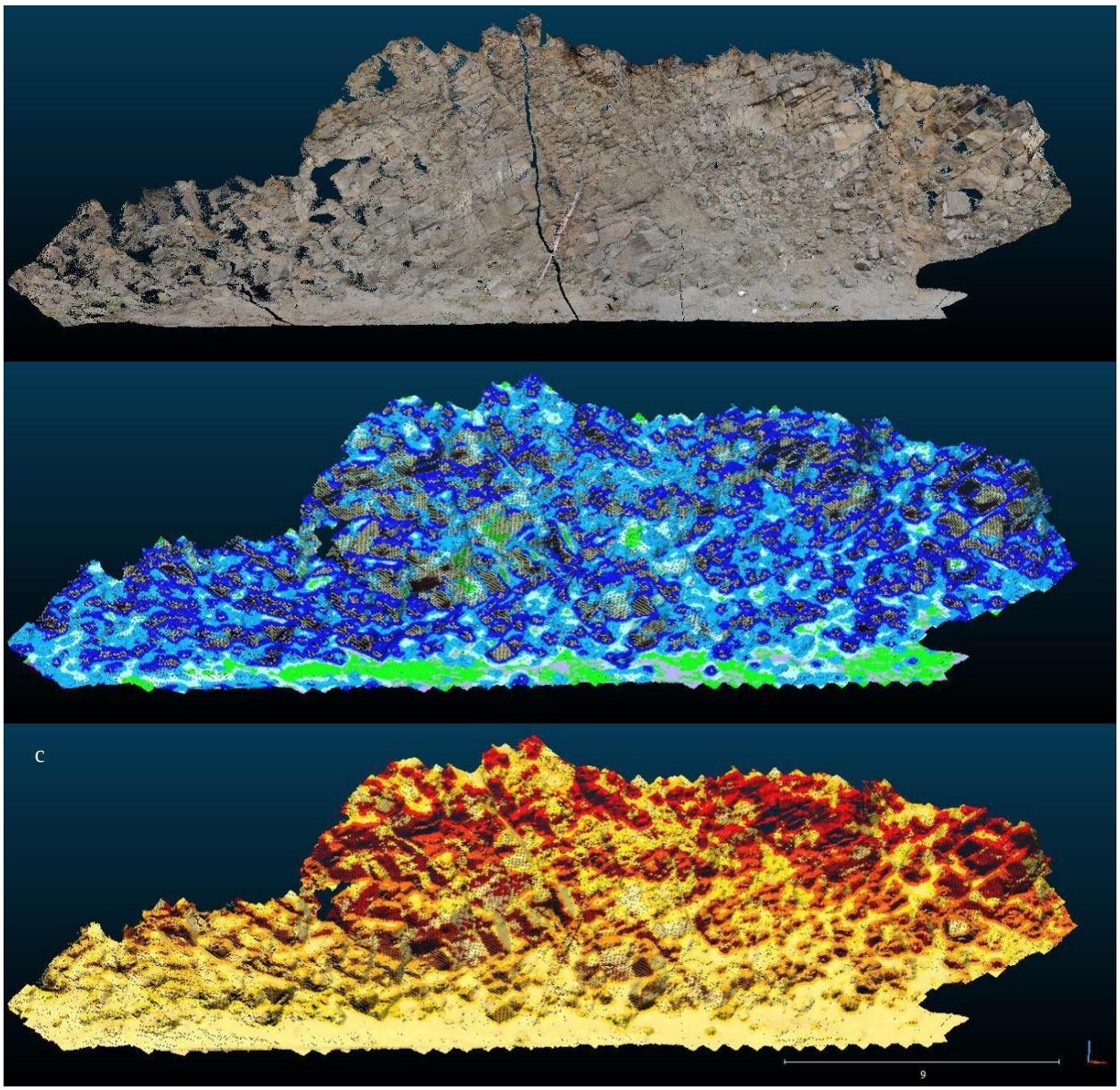

Figure 25 MP 85.5 of Glenn Highway: a) lidar point cloud data, b) RAI classified cloud and c) RAI hazard rating. Note the small black sections are areas where there are holes in the coverage due to shadows and lidar scanner position.

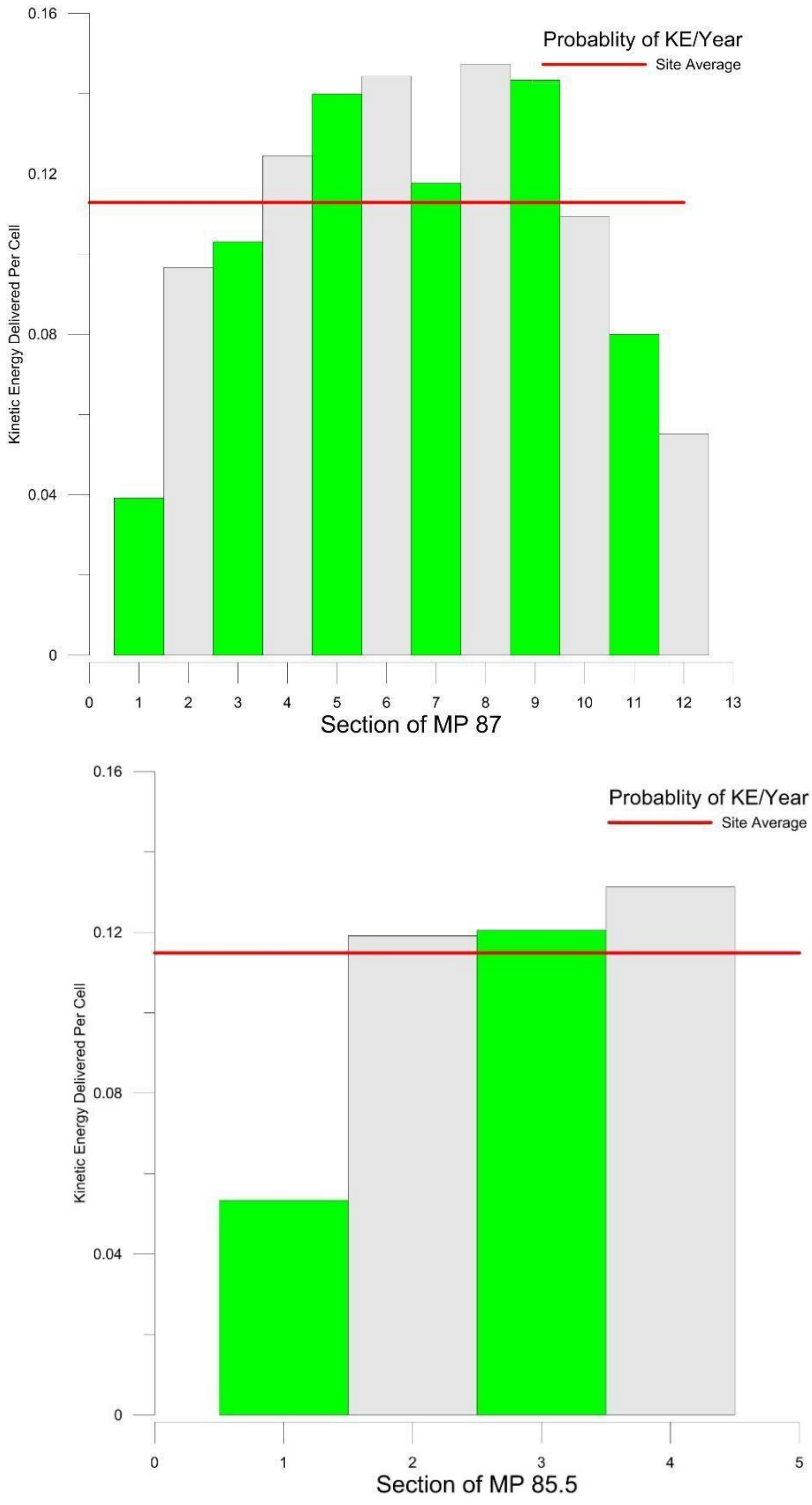

Figure 26: Energy cell segments: a) section 87 and b) section 85.5 are split into 10 m segments and the energy per cell is calculated for each segment. The red line is the site average.

Chapter 5: Discussion

A long-term concern of highway managers is unstable slopes (e.g., rockfalls or landslides) along transportation corridors. Instabilities create safety risks and impact regional commerce, even if events occur infrequently. The infrequency of slope movement often results in complacency, especially with respect to budgeting for preventative solutions. Coupled with laborious and costly monitoring of slopes over time, it is understandable that most decision support systems that would support proactive transportation asset management (TAM) initiatives have not been implemented.

Current landslide inventory systems require significant time to develop and generally provide limited information after a collapse has occurred. As such, they do not provide an understanding of how risk varies with time and location. A proactive, near-automated approach for the identification of slope instability offers the potential to enhance public safety while simultaneously reducing overall operation and repair costs and the economic consequences of interrupted transportation and commerce.

Remote sensing technology, such as lidar (light detection and ranging) laser scanning, shows promise for the rapid assessment of linearly distributed infrastructure systems such as highways. Time-series lidar datasets enable a higher level of quantitative asset management confidence than current probabilistic studies based on landslide inventories.

The first phase of this project summarized in the previous report focuses on the development of a quantitative risk model for slope stability assessment using terrain models created from lidar data. In the second phase of the work, we have focused on quantitative time-series analysis using lidar data and integrating this information into the model developed from the first phase of research as well as into a transportation agency's asset/performance

management program. The RAI classification provides a unique ability to find problem areas and quantify potential risk in a metric with a physical meaning. Using change detection from time series data and morphological indices derived from point clouds, the RAI uses advancing technology to the advantage of the owner becoming a valuable tool in the hand of asset managers allowing exploration of potential hazard at different levels. Inventory systems that take valuable time to develop can be reduced to the processing of point clouds which can also be used in other asset management functions. The processing for the RAI can be added for a low cost onto point clouds acquired for other purposes, or can be a good starting point to a geotechnical asset management program that can include other analysis using the point clouds to improve decision making processes and save time and money. The importance of a classification system is to provide comparison amongst sites such that decisions can be made to improve safety and mitigate problems. The RAI provides this structure for comparison of sites, but it also provides valuable spatial resolution that field mapped classification systems lack. This spatial resolution can improve design, mitigation and overall safety of transportation networks.

In addition to the rock slope classification techniques and change detection developed herein, a key value to lidar is the ability to use a single dataset multiple times. Additional opportunities that lidar can help support and inform for asset management could include environmental impacts (e.g., erosional deposits and sediment flux into streams), road safety impacts (e.g., loss of shoulder width due to rockfalls), hydrologic impacts (e.g., cluttering of ditches used for road drainage with debris), and maintenance (e.g., the amount of material maintenance needs to remove annually). Repeat lidar surveys provide both quantity (volumes and rates of changes) and location information that can be important to determine high priority areas and allocation of limited resources. This information can be provided in a much more

effective, efficient, and objective manner than reports from maintenance crews who can only provide relative estimates and often do not have sufficient time to be burdened with determining and reporting this information. Ultimately, this information can then be transformed to document costs over time and project maintenance costs in the future. This will then help inform decisions related to the potential effectiveness and benefits of installing various types of improvements at specific sites in the corridor.

Note there are also a variety of other applications that can be supported by mobile lidar data related to asset management such as geospatial inventories of sign, pole, and other features. These are summarized in the phase I report as well as in the TRB mobile lidar guidelines (Olsen et al. 2013).

Chapter 6: Recommendations

The goal of the PacTrans Phase I project was to develop a qualitative relative risk model for slope stability assessment using terrain models created from MLS data. Phase II focused on a quantitative, time-series analysis using MLS data and integrating this information into the qualitative model developed during Phase I.

Quantitative and qualitative risk modeling enable administrators to evaluate slope assets along highway corridors and determine risks. This workflow identifies a slope's susceptibility to failure using GIS-based data and state-of-the-art mobile mapping technologies, resulting in a virtual 3D digital corridor map indicating slope stability in unprecedented detail. The developed classification scheme and processing tools are invaluable to administrators tasked with managing a corridor slope inventory. This effort can directly be tied into an agency's transportation asset\performance management program.

As a result of this project, DOTs will be able to make predictions of the likelihood of slope failure and resulting socio-economic impact, thereby allowing proactive planning and execution of slope remediation projects. This objective approach will allow effective communication of transportation infrastructure budget impacts to decision makers including DOTs, legislatures, and state executives. The platform is a tool for objectively identifying which rock slopes pose the greatest risk to a transportation corridor and the customers that use it – thereby indicating where limited resources may be allocated so as to ensure the greatest benefit to a highway corridor and the transportation system as a whole. Proactive slope remediation allows for a cost-effective approach, but more importantly, is a means to mitigate life-safety concerns posed by slope failures. Thus, the public, as both user and taxpayer, will benefit from this project.

The end product of this project is a detailed methodology and supporting tools in which a DOT could take the output from a geo-referenced MLS survey (e.g., las file) and semi-automatically generate products such as a terrain model, slope map, curvature map, slope stability analysis map (e.g. RAI), change/deformation analysis map, etc. with minimal input from the end-user. These products can be read into software commonly available to DOT such as GIS and open source software such as *CloudCompare*.

Recommendations from this phase of research include:

1. Collect repeat mobile lidar surveys along highways with steep natural or cut slopes as part of a broader asset management program for reduced costs. When collecting mobile lidar data for an area, ensure that the accuracy (<5cm 3D RMS) and resolution (2-3cm spacing between points) requirements are sufficient in areas requiring rock slope analysis. These can be relaxed in other areas as long as the data is not needed for other applications that require higher accuracy.
2. The temporal frequency of scanning should match the level of activity along the corridor commonly observed. Highly active sections of corridors may require surveys as frequently as monthly, seasonally, or annually. Less active sections could be surveyed less frequently such as every five years. These can then be adjusted based on the results of the change detection. Hence, it will be an iterative process based on the findings of the previous survey.
3. Select sites with very high activity should be scanned with static lidar to enable improved coverage, resolution, and accuracy of the slope for analysis. Additionally, mobile lidar can be supplemented by strategically located terrestrial laser scans.

4. Fusing mobile or static terrestrial lidar with airborne lidar data can also be important to understand the bigger picture of what is happening farther from the roadway.
5. Other technologies such as unmanned aircraft systems (UAS) may help provide a better view of the tops of the slope because they can be positioned from a variety of locations. Static lidar is often limited to the shoulder of the road, which limits the view of the upper portions of the cliff.
6. Data management practices such as those described in the Transportation Research Board (TRB) mobile lidar guidelines (Olsen et al. 2013) should consider the importance of repeat scans and legacy data that should be preserved for longer term studies and evaluations of change at sites along the highway corridors. Such practices will help ensure longevity to the data and increased value from its repeated use.

APPENDIX A Lidar RAI Calculation Program

Input and Output Parameters

This appendix provides basic information on using the RAI hazard rating program, including its input and output parameters.

To run, ASCII text files in the format XYZRGBI, XYZI, or XYZ are dragged and dropped into the binary converter. Once the file is converted to a binary format (.bpd), the bpd file is dragged and dropped into the program. A file options.txt, which can be opened in a basic text editor, enables the user to change various options. These input parameters are summarized in Table A-1. Table A-1 also provides recommended values when data are collected in a similar fashion to that described in this report.

Table A-2 provides an overview of the various files output by the program. Notably, the program exports a texture mapped surface model (obj file), ground filtered points, and a point cloud dataset with various attributes including slope, surface roughness, RAI classification, and RAI hazard rating. The full range of attributes in this text file are summarized in Table A-3. The text file is best viewed in *CloudCompare*, which can display each attribute one at a time. Note that no data values vary between parameters and the display range of *CloudCompare* needs to be adjusted to the actual range of the data.

Table A-1 Summary of input parameters and recommended values

Parameter	Type	Typical Values	Description
Cell Size	Double	0.05 to 0.20 m	The desired cell size for the dataset. Typically 0.05 m for static lidar, higher for mobile
Minimum # points per cell	Int	>= 1	Minimum number of points per cell to use that cell in further calculations. Data in cells with less than this number of points are ignored.
Roughness Window Size	Int	10	Number of Roughness Window Sizes. Starting with a roughness window size 1= 1 neighbour in each direction (3x3 grid), 2= 2 neighbours in each direction (e.g, 5x5 grid), … n= n neighbors in each direction (e.g., (n+1)x(n+1) grid).
Fill Holes	Int	1	Fill Holes by interpolating values in cells with no data using a thin plate spline fit through centroid points in neighboring cells. (0 = no hole filling, 1= fill holes for both datasets, 2 = fill holes for the baseline dataset only in the case of Change Analysis).
Hole Fill Window	Int	10	The window size to search for points to fill holes. 10=a 10x10 window.
Percent Points in Window	Double	0.25	The percent of cells in the window that are required to have data meeting the minimum point requirement in order to fill adjacent holes. Higher values mean that holes are not filled in sparse areas with missing data.
Regularization	Double	0	The regularization parameter to relax the thin plate spline interpolation. Larger values mean less curvature.
Rotate Points	Int	1	1= Rotate data so that the best fit plane of the dataset is aligned with the XY plane. This improves triangulation on the cliff face. 0 = no rotation and the triangulation and analysis is done in the XY plane.
RDA Analysis	Int	0	Flag to determine if the code will perform RDA analysis. 0 = no, 1= yes. This requires files with extensions of (_A,_F,_G,_W) where those parameters of aperture, fracturing, geology, and weathering have been
Change Analysis	Int	1	Flat to determine if Change Analysis will be performed. 0= no, 1= yes. Requires a second dataset from an earlier epoch with extension of _BL for a baseline.
Change Smoothing Window Size	Int	2	Change Smoothing window size for individual failure identification. Higher values smooth the change values to create larger clusters. Larger values result in smaller, more sporadic clusters.
Significant Change Threshold	Int	0.05 to 0.10 m	The threshold value of what indicates detectable change. Dependent on the georeferencing quality of data.
Remove average bias	Int	1	1 = Remove average bias between scans. This can help remove effects of georeferencing error. (WARNING - COULD REMOVE UNIFORM CHANGE ACROSS THE SITE!!!!)
RAI slope classification	int	1	1= perform the RAI classification and analysis. 0 = RAI analysis not performed.
REI Probability	Double	0.05	REI PROBABILITY VALUE-No longer used, but don't delete the field yet.
Specific Gravity	Double	2.7	The specific gravity value desired for mass calcualtions
Ground Filter	Int	1	1= Run the ground filter to remove vegetation. Outputs a subset of the points with an extension of _GRND before completing the rest of the
GF Iterations	Int	5	The number of iterations of the ground filter to complete.
GF Coarse Cell Size	Double	1.0	The cell size to start the ground filter with. Each iteration reduces the cell size linearly until the desired cell size (first variable) is reached.
GF coarse threshold	Double	1	Threshold factor of points to keep in the ground model for coarse analysis. Multiplied by cell size.
GF fine threshold	Double	3	Threshold factor of points to keep in the ground model for fine analysis. Multiplied by cell size.
GF coarse median filter WS	Int	1	Window size for the median filter of the coarse ground model
GF fine median filter WS	Int	5	Window size for the median filter of the fine ground model. Larger value will result in more smoothing and less noise
Export PTX	Int	1	1 = export a ptx file (organized scan grid) and associated png of color map for the cliff.

Table A-2 Various output files produced by the RAI hazard rating program.

OUTPUT FILE	DESCRIPTION
bpd	Input file after running the binary converter for a text file that has X,Y,Z or X,Y,Z,R,G,B, or X,Y,Z,R,G,B,I values.
_GRND.bpd	Output file when running ground filter that only contains a subset of the points.
obj	3D triangulated surface model of the data points. This includes verticies, facets, texture mapping, and normal information.
png	Texture map image for the 3D triangulated surface model with RGB color values
mtl	A material file to support the texture map for the obj file
ptx	An export of the centroids for each cell as if they were acquired on an organized scan grid in rows and columns
_PARAMS.txt	The master output file with the parameters described in table X.
_FIDvolsPOS.csv	An output file with the IDs, volumes, and dominate RAI class for each accretion cluster
_FIDvolsNEG.csv	An output file with the IDs, volumes, and dominate RAI class for each erosion cluster
_CLASSAREAS.txt	Area calculations (e.g., m^2 for each RAI class on the slope). 7 = unclassified, 8 = total area. This output file also provides failure rate for each RAI class (the number of cells that have failed for each RAI class, the total number of cells within each RAI class, and the percent failed).
f0_GRNDCF.bil, .hdr, .stx	Grid files of the ground model in BIL format. (Note that they are in the direction of the best fit plane). The numbers correspond to the iteration. F is after median filtering, u is before. The hdr and stx files are needed for the bil format and are header and statistics files, respectively.
_PARAMSSTATS.csv	Summary statistics of many of the parameters in the PARAMS.txt file.

Note that each file is created to append and change the extension of the name of the input file.

For example, if the input file is GG10C.bpd, the ground filtered points would be

GG10C_GRND.bpd.

Table A-3 Output parameter fields of the RAI processing program

Fields	Description
X,Y,Z	X,Y,Z coordinates of the centroid of the lidar points in each cell, typically in m
R,G,B	Average Red, Green, Blue color values (0-255) of all lidar points in each cell.
Intensity	Average intensity value of all lidar points in each cell
SlopeDEG	The local slope of each cell, in degrees
SlopeRAD	The local slope of each cell in radians
NX,NY,NZ	The normal vector components of the surface in each cell, based on its connectivity with neighbors
Rel_Z	The height of the cell above the base of cliff
RoughDEGXX	Roughness values for a window size of XX in degrees. Roughness values are determined as the standard deviation of slope within a window. For example, RoughDEG01 means that the roughness values is evaluated for a cell by looking at cells that are 1 cell away from the current cell. (e.g, a 3x3 window).
CRVX	For diagnostics only. Curvature in the X direction of the local, rotated coordinate system.
CRVY	For diagnostics only. Curvature in the Y direction of the local, rotated coordinate system.
CRVXY	Local curvature for each cell
Area	The 3D surface area connecting the centroid point of a cell with its neighboring cells.
CHG	The 1D magnitude of change in the direction of the best fit plane of the dataset (i.e. orthogonal to the general cliff surface). The units are the same as the input data, typically in meters. Positive values indicate accretion, negative values indicate erosion.
VOL	The change in volume of each cell between datasets. The units are the cube of the input data units (e.g. m^3). Positive values indicate accretion, negative values indicate erosion.
SIG_CHG	An indication if the observed change is larger (either positive or negative) than a threshold value to remove effects of georeferencing error. +1 means significant accretion was observed, -1 indicates significant erosion occurred, and 0 means that the difference was not significant (i.e., within +/- the
FID_NEG	The ID for the cluster of erosion which the cell belongs to. 0 indicates that there was no significant erosion in the cell.
FID_POS	The ID for the cluster of accretion which the cell belongs to. 0 indicates that there was no significant accretion in the cell.
KE	The computed kinetic energy for the cell, in Joules
REI	The rockfall energy index (REI) for the cell
RAI	The RAI classificaiton for the cell. UNCLASSIFIED = 0, TALUS=1, MASSIVE_STABLE=2, SMALL_ACTIVE=3, MEDIUM_ACTIVE=4, LARGE_ACTIVE=5, SHALLOW_OVERHANG=6, FLAT_OVERHANG=7.
RAIclusterPOS	The general RAI classificaiton for the accretion cluster that the cell belongs to. -1 indicates that it is not applicable.
RAIclusterNEG	The general RAI classificaiton for the erosion cluster that the cell belongs to. -1 indicates that it is not applicable.

APPENDIX B RAI Site Visualizations

This appendix contains graphics showing the application of the RAI algorithm to several sites in Glitter Gulch and Long Lake. Figure B-1 shows the locations of each study site within Alaska as well as the cumulative Kinetic Energy Potential for each site. Figure B-2 shows the point clouds, the RAI classification, and RAI Hazard Rating for each site.

The presented figures show the ability of the RAI classification and hazard rating to provide information across a wide range of scales from a local level (5cm resolution in Figure B-2) with high detail to larger areas (e.g., segments of a corridor in Figure B-1) where the information can be used to prioritize sites for mitigation or further study.

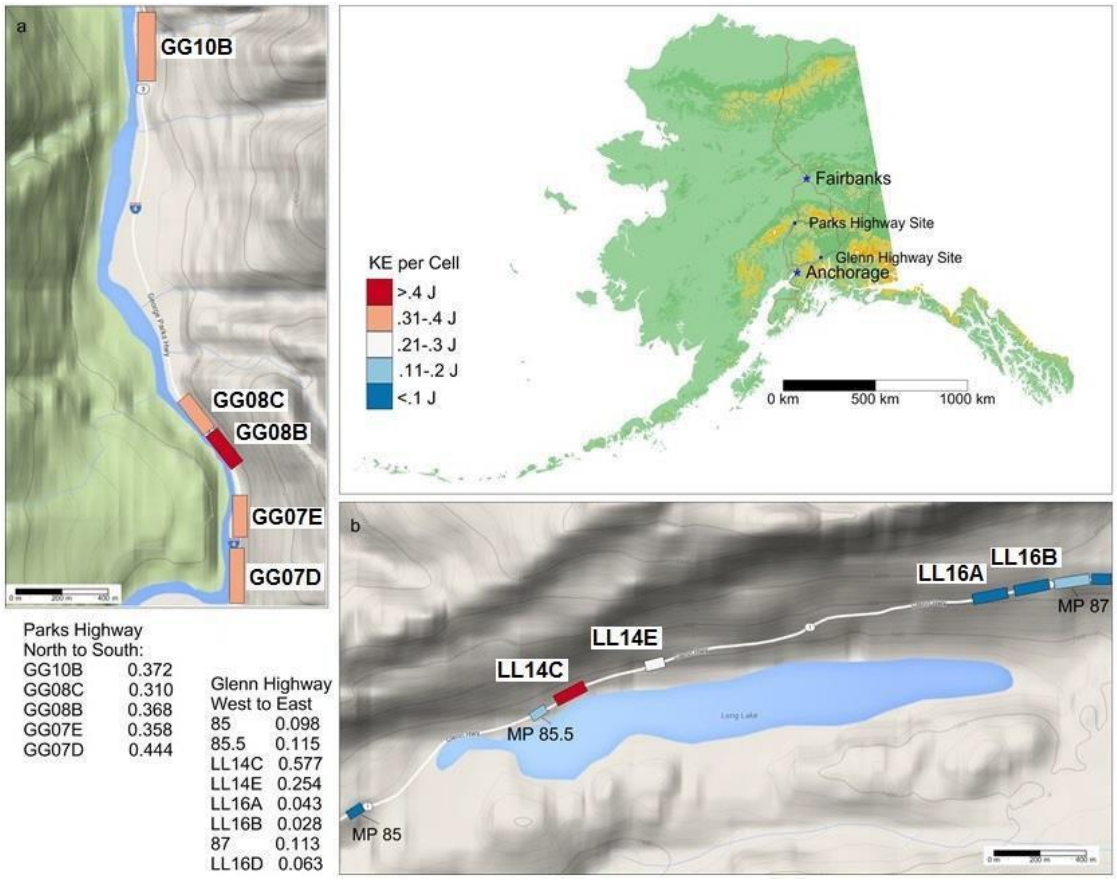

Figure B-1 Site map showing location of study sites along the highways in Glitter Gulch (GG) and Long Lake (LL) in Alaska. The total Kinetic Energy (KE) for each site/cell is shown, highlighting locations with higher levels of activity.

Table B-1 Point clouds, RAI classification and RAI hazard ratings for individual sites

	Parks Highway – North to South
GG10B Top) Lidar Point Cloud (intensity shaded) Middle) RAI Classification Bottom) RAI Hazard Rating	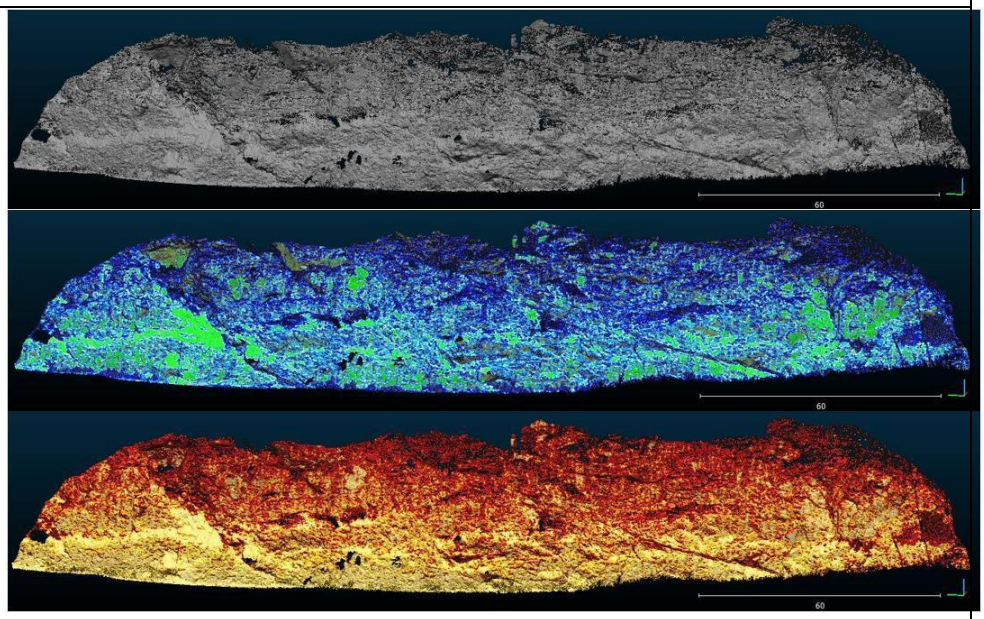

GG08C Top) Lidar Point Cloud (intensity shaded) Middle) RAI Classification Bottom) RAI Hazard Rating	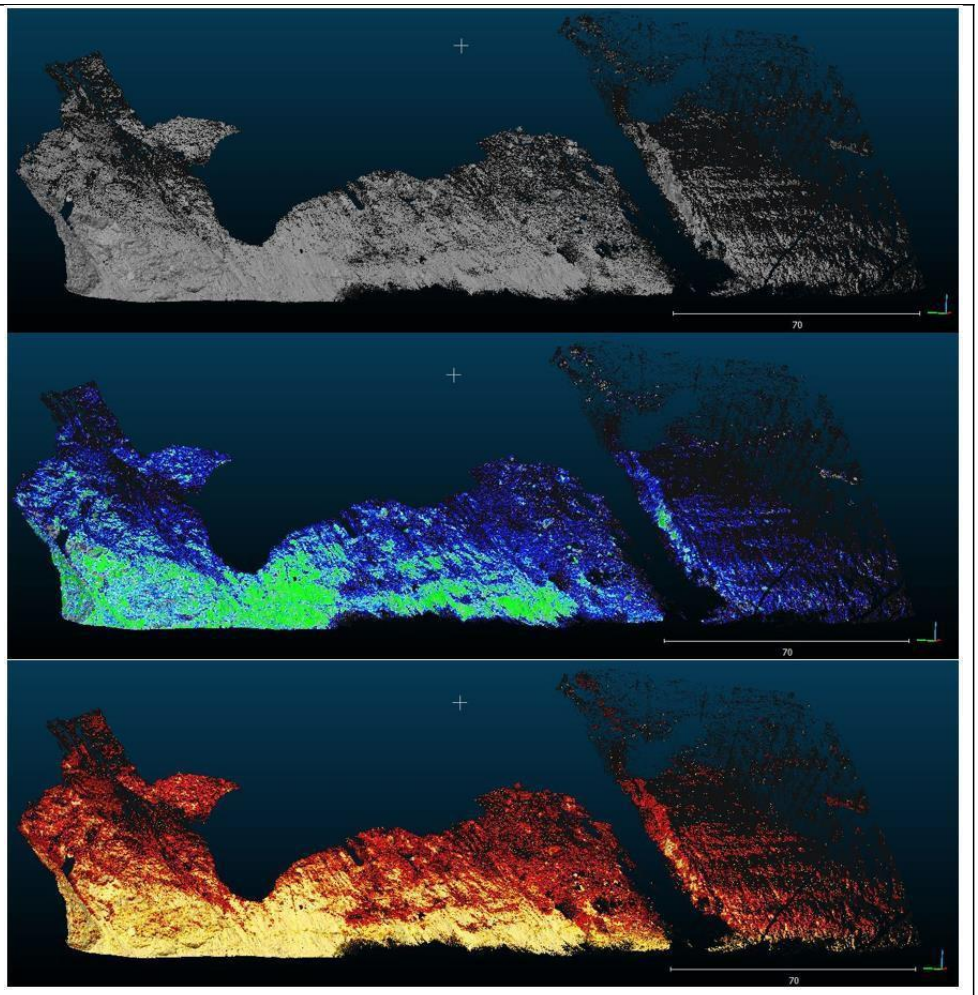

GG08B Top) Lidar Point Cloud (RGB color) Middle) RAI Classification Bottom) RAI Hazard Rating	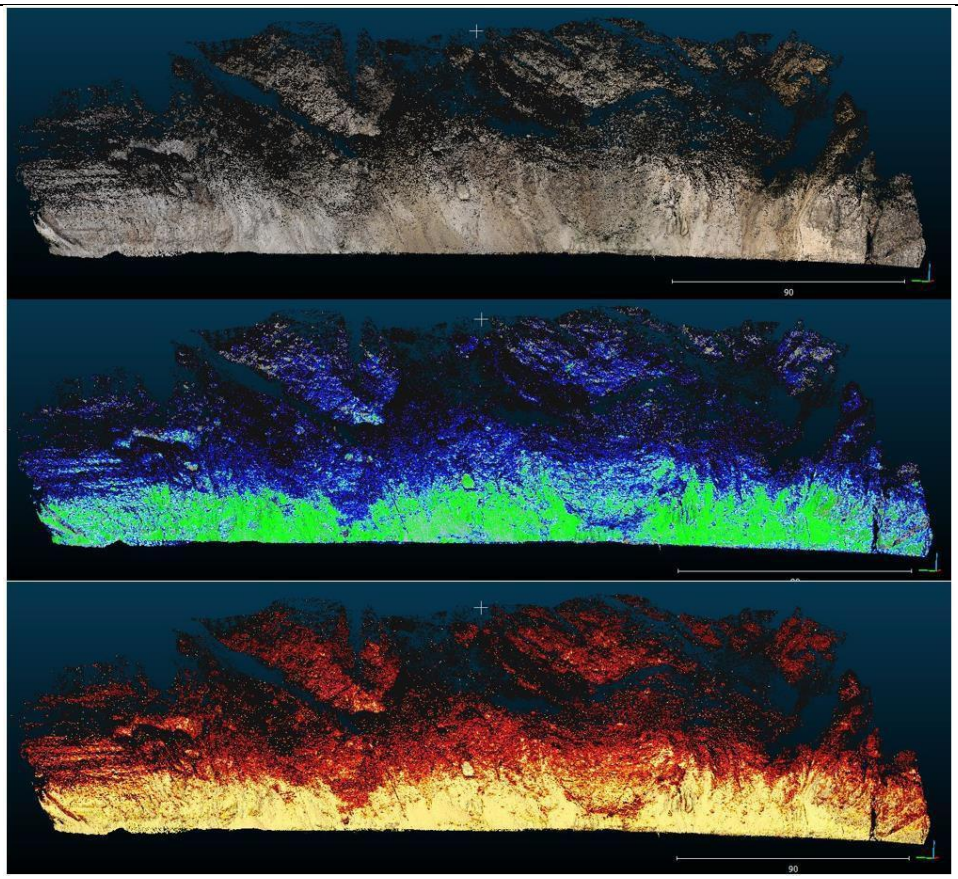
GG07E Top) Lidar Point Cloud (RGB color) Middle) RAI Classification Bottom) RAI Hazard Rating	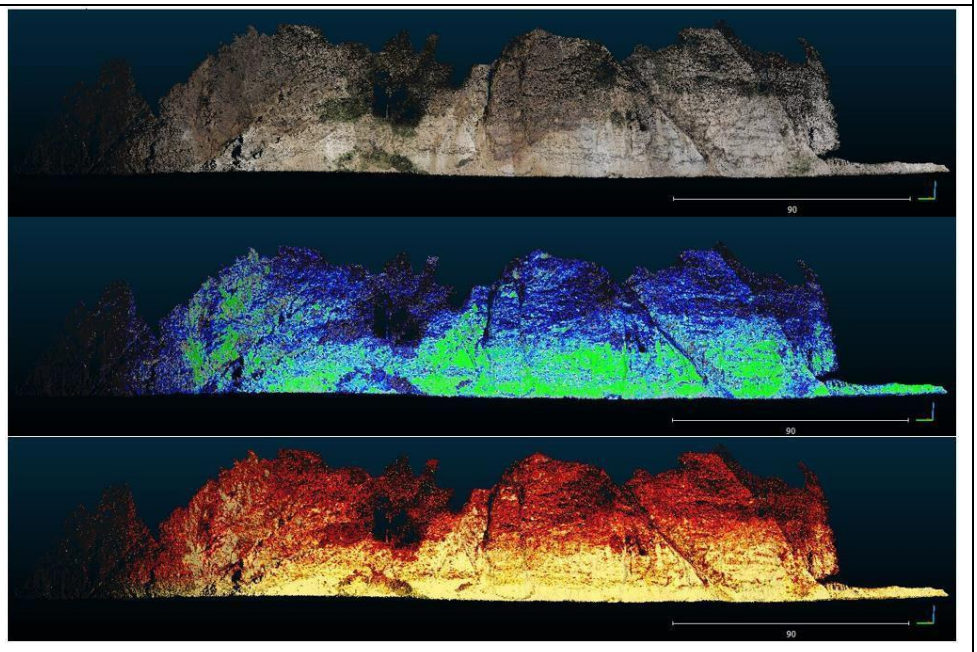

GG07D Top) Lidar Point Cloud (RGB color) Middle) RAI Classification Bottom) RAI Hazard Rating	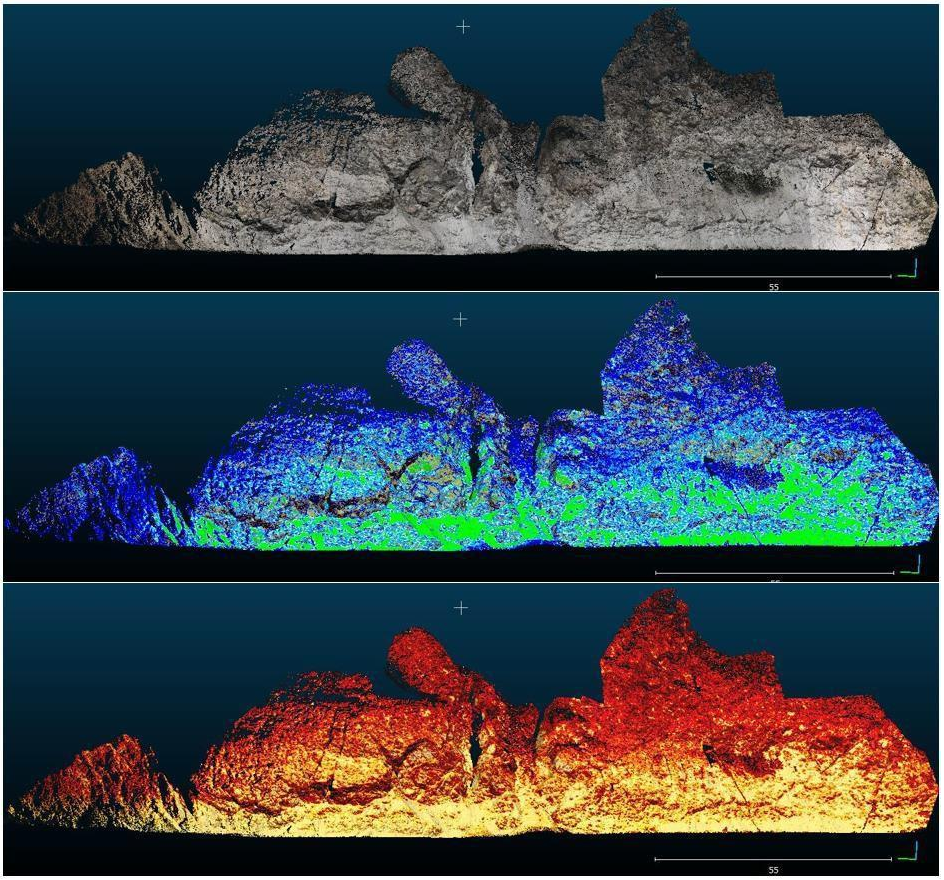

	Glenn Highway – West to East
LL14C Left) Lidar Point Cloud (RGB color) Middle) RAI Classification Right) RAI Hazard Rating	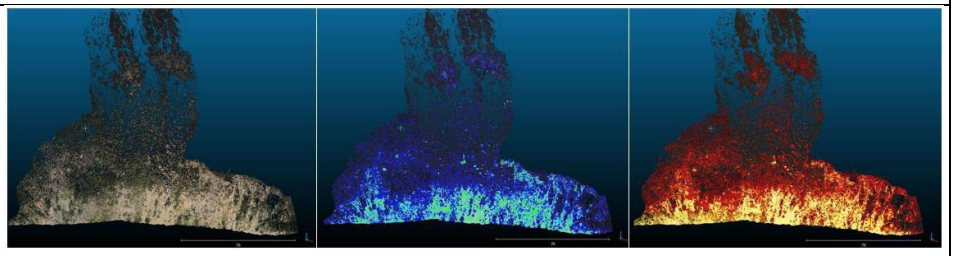

LL14E Top) Lidar Point Cloud (RGB color) Middle) RAI Classification Bottom) RAI Hazard Rating	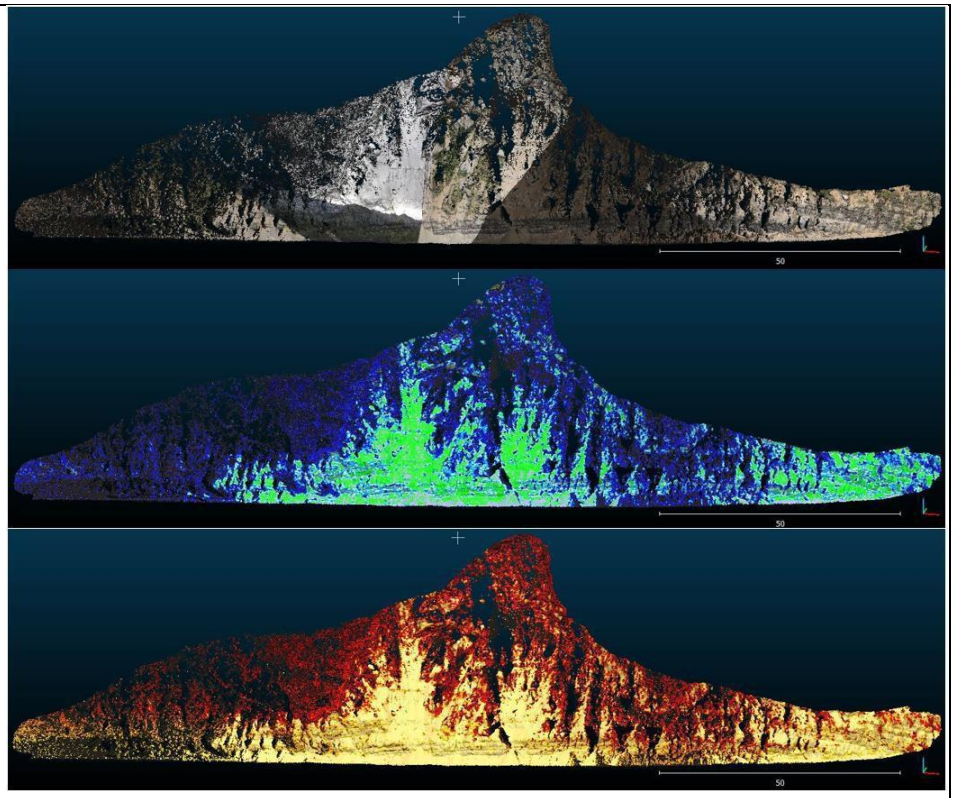
LL16A Top) Lidar Point Cloud (RGB color) Middle) RAI Classification Bottom) RAI Hazard Rating	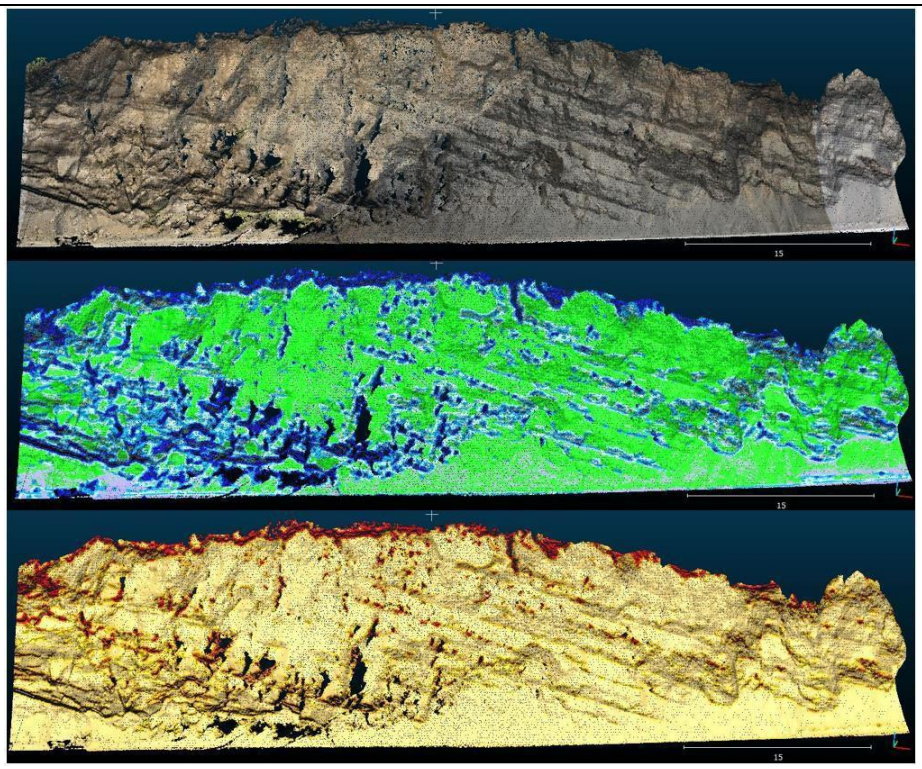

LL16B Top) Lidar Point Cloud (intensity shaded) Middle) RAI Classification Bottom) RAI Hazard Rating	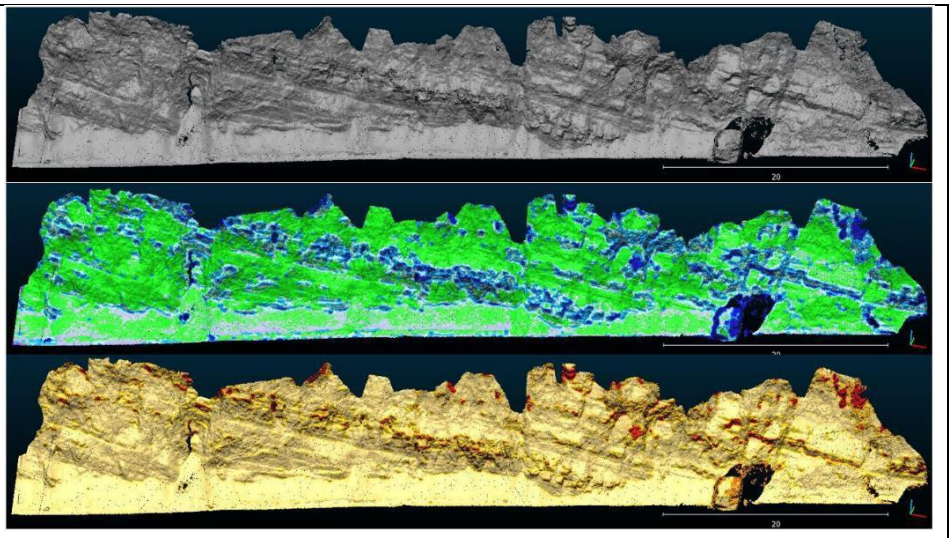
LL16D Top) Lidar Point Cloud (RGB color) Middle) RAI Classification Bottom) RAI Hazard Rating